Active tectonics in Eastern Lunana (NW Bhutan): Implications for the seismic and glacial hazard potential of the Bhutan Himalaya

M. C. Meyer,[1] G. Wiesmayr,[2] M. Brauner,[3] H. Häusler,[2] and D. Wangda[4]

[1] Paleoseismological investigations, brittle fault analysis, and paleostrain calculations combined with the interpretation of satellite imagery and flood wave modeling were used to investigate the seismic and associated glacial hazard potential in Eastern Lunana, a remote area in NW Bhutan. Seismically induced liquefaction features, cracked pebbles, and a surface rupture of about 6.8 km length constrain the occurrence of $M \geq 6$ earthquakes within this high-altitude periglacial environment, which are the strongest earthquakes ever been reported for the Kingdom of Bhutan. Seismicity occurs along conjugate sets of faults trending NE-SW to NNW-SSE by strike-slip and normal faulting mechanism indicating E-W extension and N-S shortening. The strain field for these conjugate sets of active faults is consistent with widespread observations of young E-W expansion throughout southern Tibet and the north Himalaya. We expect, however, that N-S trending active strike-slip faults may even reach much farther to the south, at least into southern Bhutan. Numerous glacial lakes exist in the investigation area, and today more than 100×10^6 m^3 of water are stored in moraine-dammed and supraglacial lakes which are crosscut by active faults. Strong earthquakes may trigger glacial lake outburst floods, and the impact of such flash floods may be worst 80 km downstream where the valley is broad and densely populated. Consequently, tectonic models of active deformation have to be closely linked with glacial hazard evaluation and require rethinking and modification. **Citation:** Meyer, M. C., G. Wiesmayr, M. Brauner, H. Häusler, and D. Wangda (2006), Active tectonics in Eastern Lunana (NW Bhutan): Implications for the seismic and glacial hazard potential of the Bhutan Himalaya, *Tectonics*, *25*, TC3001, doi:10.1029/2005TC001858.

1. Introduction

[2] One of the most striking features of the Himalayan orogen is the first-order along-strike continuity of major faults and tectonostratigraphic units that are traceable over an approximately E-W distance of 2500 km. From the southern most frontal part of the orogen toward the Tibetan Plateau in the north, these major features include the Main Frontal Thrust, the Main Boundary Thrust, the Lesser Himalayan Sequence, the Main Central Thrust (MCT), the Higher Himalayan Crystalline (HHC), the South Tibetan Detachment System (STDS), Tethyan Sedimentary Sequence (TSS) and the Indus Yarlung Suture (Figure 1).

[3] It is generally recognized that the Himalayan orogen grew along south directed and southward propagating crustal-scale thrust imbricates since the Eocene [e.g., *Le Fort*, 1975; *Searle et al.*, 1987; *Dewey et al.*, 1988; *Hodges*, 2000, and references cited therein; *Stüwe and Foster*, 2001]. Today about 80% of recent convergence between the Indian and Asian crustal plates are taken up mainly by thrusting kinematics in an orogen-normal direction along the Himalayan frontal thrust [*Bilham et al.*, 2001; *Jackson and Bilham*, 1994]. These thrusts are supposed to join into a common detachment in depth, into the gently north dipping Main Himalayan thrust [*Nelson and Project INDEPTH Team*, 1996]. In addition to these thrusting kinematics, two types of extensional structures significantly contributed to the tectonic evolution of the orogen. The first is the STDS [*Burg and Chen*, 1984; *Burchfiel et al.*, 1992], a system of shallowly north dipping normal faults, which acted contemporaneously with the Main Central Thrust during the Miocene southward extrusion of the HHC. The second type comprises ESE-WNW directed extension of the Tibetan Plateau and resulted in both normal faulting (N-S trending rift systems) and NW-SE and NE-SW oriented conjugate strike-slip faulting (Figure 1) [*Armijo et al.*, 1986, 1989; *Fielding et al.*, 1994; *Cogan et al.*, 1998]. Seismic moment tensors for earthquakes within northern and central Tibet suggest that ESE-WNW extensional strain dominates active deformation of the plateau interior, [e.g., *Molnar and Lyon-Caen*, 1989; *Langin et al.*, 2003, and references cited therein] which causes an eastward movement of crustal material out of India's path. Between 79°E and 93°E eastward stretching amounts to 21.6 ± 2.5 mm/yr [*Zhang et al.*, 2004].

[1]Institute of Geology and Paleontology, University of Innsbruck, Innsbruck, Austria.
[2]Department of Geological Sciences, University of Vienna, Vienna, Austria.
[3]Geoexpert Research and Planning Gmbh, Vienna, Austria.
[4]Geological Survey of Bhutan, Ministry of Trade and Industry, Thimphu, Bhutan.
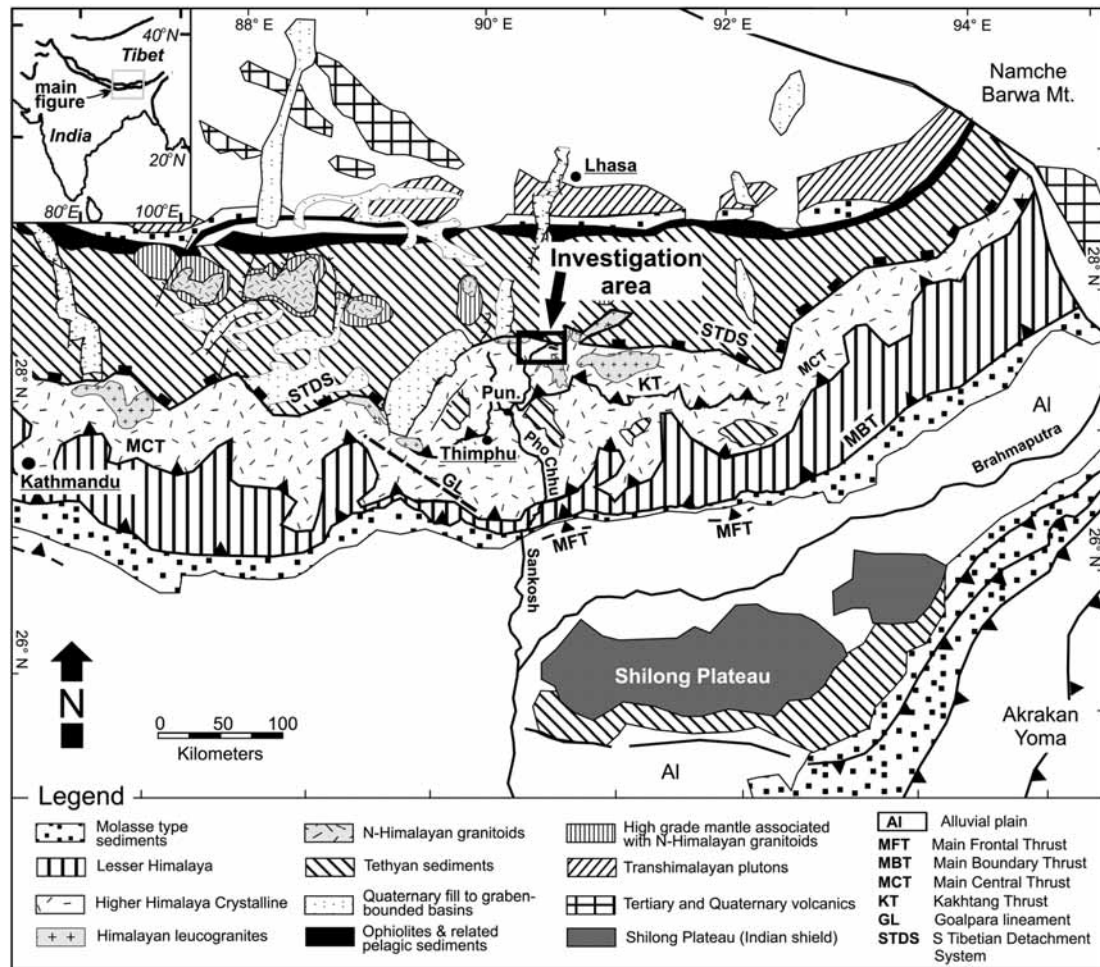
Figure 1. Geological and tectonic overview of the east Himalaya and the Shilong plateau. Compiled after *Gansser* [1983], *Cogan et al.* [1998], *Grujic et al.* [1996], *Burg and Chen* [1984], *Burchfiel et al.* [1992], and *Edwards et al.* [1999]. Seismotectonic Goalpara lineament after *De and Kayal* [2003].

[4] Despite the striking orogen-parallel continuity, complications of tectonostratigraphic units occur, especially in the Bhutan Himalayas and adjoining areas, as follows:

[5] 1. Studies on recent seismic activity in the eastern Himalaya and in Bhutan have shown that earthquakes are not only related to thrusting, but also to midcrustal to deep-crustal strike-slip faulting at a depth of 10–40 km [*Drukpa et al.*, 2006; *De and Kayal*, 2003; *Kayal et al.*, 1993; *Wu et al.*, 1998].

[6] 2. From earthquake data of the last two centuries the Bhutan Himalaya records a seismic gap within the orogen [*Bilham et al.*, 2001] (Figure 2). This gap is probably caused by the actively rising Shillong plateau located 200 km south of the Himalayan front [*Bilham and England*, 2001]. The plateau is interpreted by *Bilham and England* [2001] as an intracrustal major pop-up structure which is bounded by two steeply north and south dipping thrust faults, thus accommodating one third of the Himalayan contraction, consequently increasing the recurrence interval of great earthquakes in Bhutan bounded along the Main Himalaya Thrust and their thrust

splays and thus decreasing the seismic risk for the Kingdom of Bhutan.

[7] From our field observation and remote sensing data of Eastern Lunana (NW Bhutan) we will show that surface ruptures and liquefaction features indicate $M \geq 6$ earthquakes within the last 1 millennium in NW Bhutan which are the strongest earthquakes ever been reported for the Kingdom of Bhutan. Active deformation is confined to conjugated sets of faults which indicate E-W extension in the Tethyan Himalaya, crosscut the STDS and continue into the HHC and additionally bear a significant amount of strike-slip faulting, which have been unrecognized until now.

2. Geological Setting in Eastern Lunana

[8] The study area is located at the transition from the HHC to the TSS (Figure 3). The STDS separating these two tectonostratigraphic units is exposed on top of the steep south facing cliffs of the Table Mountains at the northern margin of the investigation area.
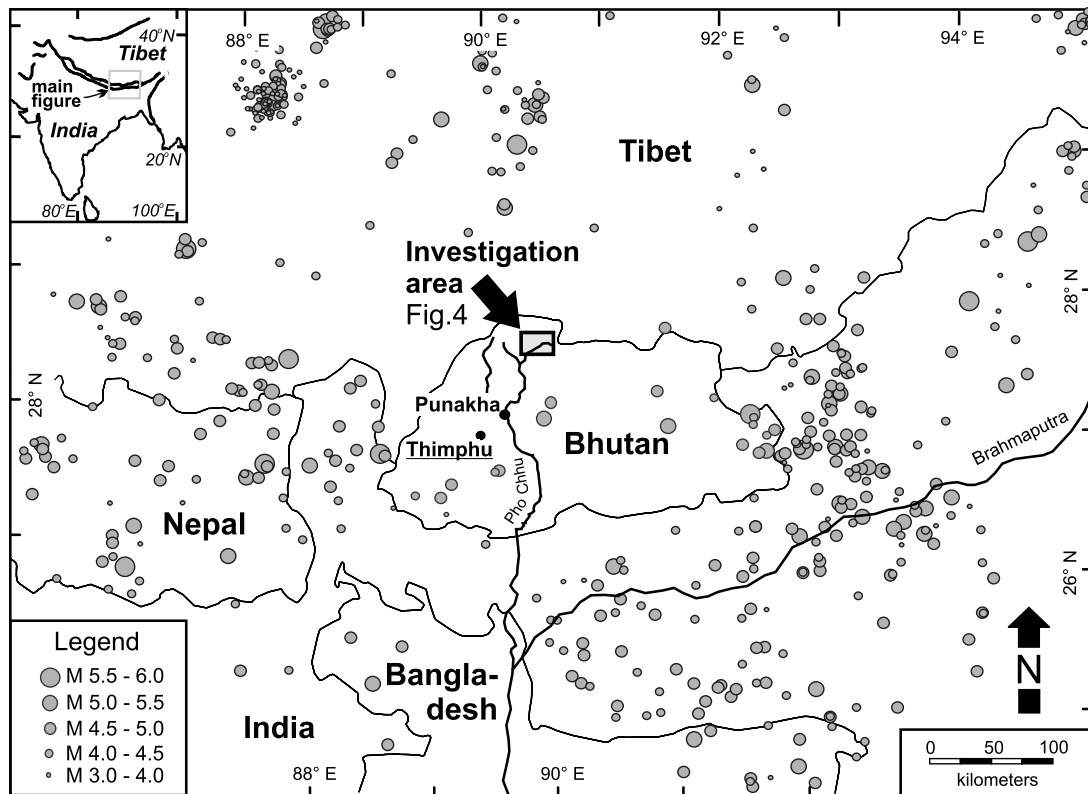
Figure 2. Seismicity of the east Himalaya and the Shilong plateau. ISC catalog 1964 to 1994. Note the deficiency of seismic events (seismic gap) within the Kingdom of Bhutan.

[9] In Lunana the HHC consists of a sequence of shallowly 10°–25° N-NNW dipping highly metamorphic sillimanite-facies gneisses and migmatites as well as leucogranites [*Gansser*, 1983; *Wiesmayr et al.*, 2002]. The leucogranites are typical Miocene Greater Himalayan leucogranites [*Gansser*, 1983; *Edwards et al.*, 1999; *Hodges*, 2000] and form major plutons, like the Khula-Kangri Pluton, the Monlokarchung-Pasalum Pluton, and the Gophu-La Pluton west and south of the study area (Figure 1).

[10] A dense network of faults postdates this plutonism (Figure 3) which can be subdivided into a first group of faults (D1) mainly defined by steeply SSE dipping oblique-slip normal faults, and by shallowly NNW dipping normal faults [*Wiesmayr et al.*, 2002]. The second group of faults (D2, Figure 3) postdates the D1 faults and is characterized by (1) NE-SW to N-S trending sinistral strike-slip faults, (2) NNW-SSE trending dextral strike-slip faults, and (3) west and east dipping normal faults. D2 faults show subhorizontal striations formed by scratching and gouging of the fault surface and partly displace Quaternary sediments.

3. Results and Discussion

[11] In this section we describe ground surface ruptures, liquefaction structures, cracked pebbles and a large landslide found in Quaternary sediments of the Tshojo, the Raphstreng, and the Thanza areas (Figure 4). The section demonstrates that based on sedimentology, morphology and the spatial association of these deformation features severe earthquake shaking and coseismic deformation is the most likely cause of these observations. Possible earthquake magnitudes, the issue of dating ground motion, regional tectonic implications and consequences for the hazard potential in the Kingdom of Bhutan are discussed afterward.

3.1. Tshojo Plain

[12] The Tshojo plain is situated at an altitude of 4050 m above sea level (asl) and was formed by the Tshojo glacier and debris flow events which both were damming the Pho river as mapped during our field surveys. The sedimentary record of the plain and preliminary radiocarbon data indicate the existence of a former lake circa 860 calibrated (cal) years B.P. which silted up by subsequent fluvial alluviation. In three places, liquefaction features within the lacustrine and fluvial sediments were found (Figure 5a).

3.1.1. Complex Convolute Folding

[13] One kilometer east of the Tshojo village, lacustrine sediments are exposed for about 30 m along the eroded river bank of the Pho river. Complex folds and convolutions are visible within a succession of massive clay with intercalated sand-silt horizons (Figure 6). We interpret the massive clay deposits as the former horizontally layered bottom sets of the Tshojo paleolake. Between two field seasons the river
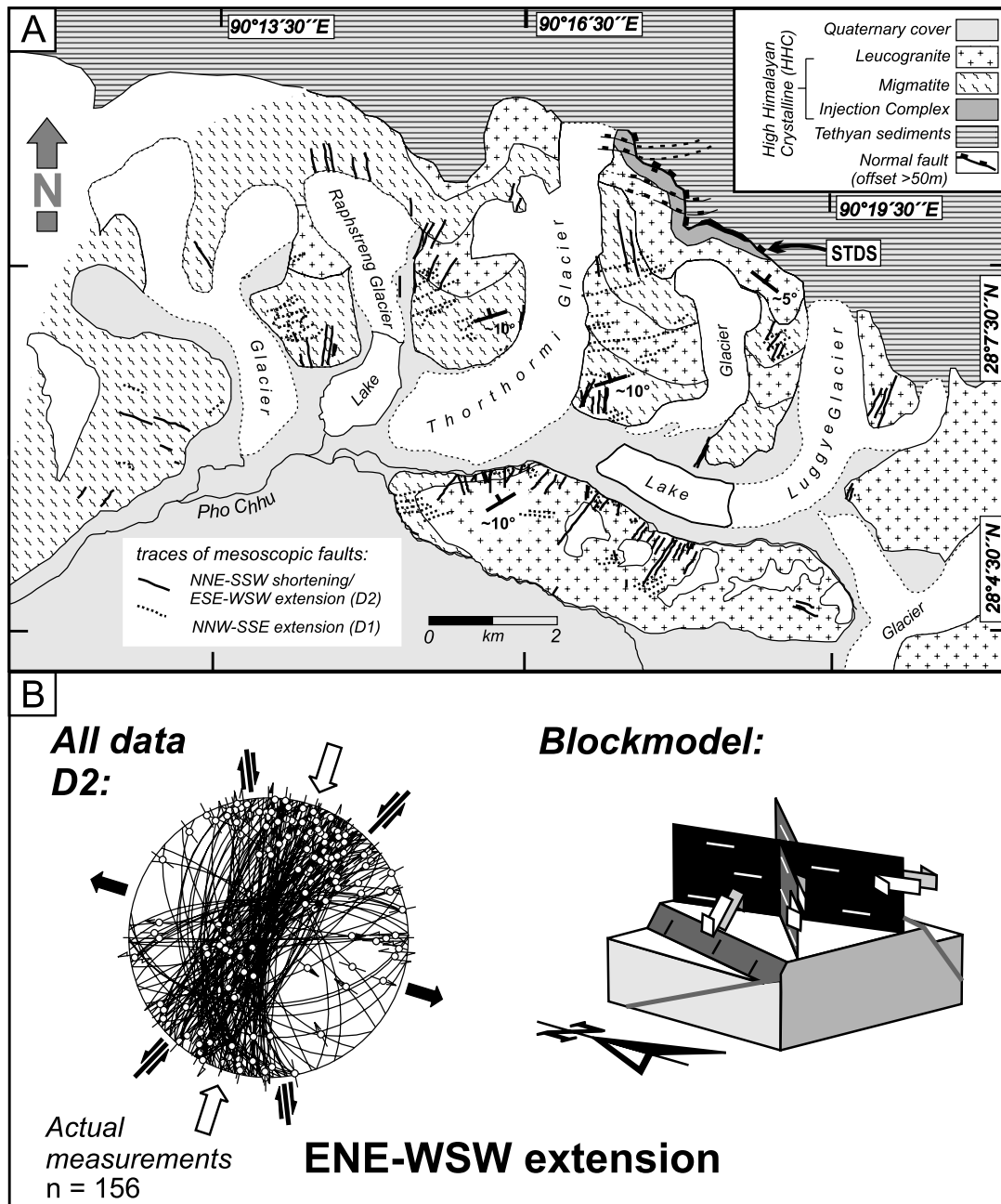
Figure 3. D2 deformation phase in Eastern Lunana. (a) Dense network of brittle D1 and D2 faults in Eastern Lunana. (b) General diagram of how the D2 fault group was generated by simultaneous strike-slip and normal faulting caused by E-W extension and N-S shortening [after *Wiesmayr et al.*, 2002].

eroded about 2–3 m of its bank and we observed intensi-fication of convolute folding with depth from gently in-clined clay deposits (year 2000) to upright fold limbs (year 2001, Figure 6b). In the original undisturbed sediment sequence coarse silt and clay was deposited on top of thick clay deposits and enclosures of sand beds between imper-meable layers were common thus establishing reverse density grading prone to liquefaction [*Brenchley and Newall*, 1972; *Potter and Pettijohn*, 1977]. An erosional discordance cut by a paleochannel and subsequent cross-bedded channel fill deposits on top of the convolute folds (Figure 6) show that the top of this outcrop was eroded during later incision of the meandering Pho river.

[14] Typical features in the outcrop situation of 2001 are highly distorted massive clays showing alternating syn-forms and antiforms with individual folds reaching up to at least 2 m in height and averaging 4 m in width. As syncline fold hinges and the transition into undisturbed
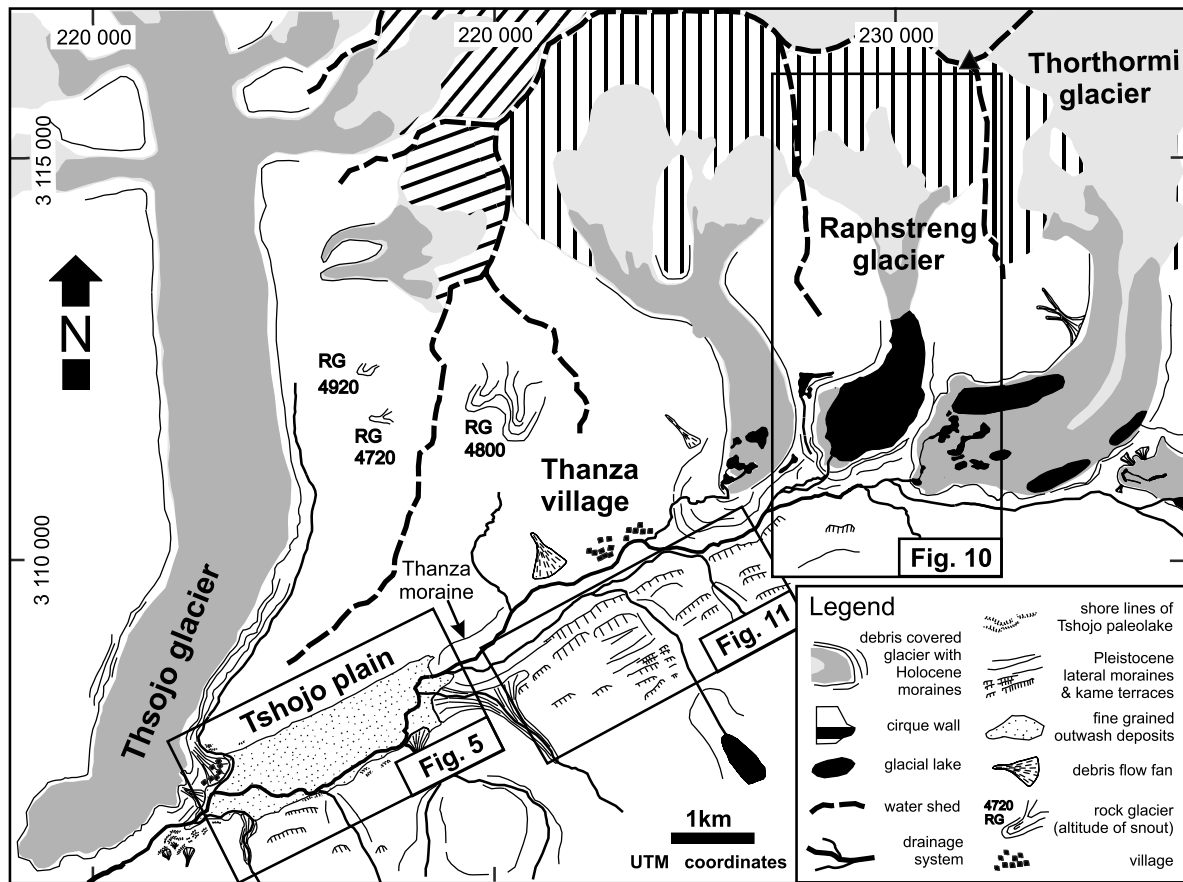
Figure 4. Geomorphological overview map of the investigation area in Eastern Lunana.

basal sediments are not exposed a fold amplitude of 2 m is regarded as a minimum thickness for the distorted horizon. Sand and silt lenses pinch and swell irregularly over decimeter to meter distances while preserving some primary sediment structures like cross bedding or horizontal lamination.

[15] The outcrop situation in 2000 showed gently inclined clay deposits and sand and silt lenses with small-scale folding and intense deformation (Figure 6b). The observed small-scale folding resembles classical convolute folds [e.g., *Lowe*, 1975; *van Loon*, 1992] but locally displays more complex geometric styles. The small-scale convolutions are characterized by highly distorted folds with irregular morphologies and sizes. Fold axial planes are slightly to strongly curved and inclined at different angles, even within the same fold (Figure 6c). Both, harmonic and disharmonic folding is common and features similar to "nappe folds" occur, where coarse sand is directly interbedded with clay, indicating stronger horizontal displacement (Figure 6d). Locally, convolute-folded silt layers are disrupted and dragged up due to vented water-sediment mixtures and water escape features with complex flame structures indicate high pore water pressures (Figure 6e). Some of the sand and silt lenses show evidence of sinking into underlying clay deposit to form an extremely amplified form of load structures known as pseudonodules, indicating originally reversed density gradients (Figure 6f) [*Mills*, 1983; *Anketell et al.*, 1970].

[16] In general, we noticed a complex folding pattern where meter-scale folds are superimposed by smaller ones. The ductile style of deformation suggests water-saturated conditions and thus liquefaction beneath or at the water table.

3.1.2. Normal Faulted Sediments and Sand Injections

[17] Faulted sediments of the Tshojo plain have been observed 1.2 km east of the complex convolute folds and 2 km east of the Tshojo village (Figure 7). A conjugate set of subvertical normal faults, trending NNW-SSE displaces horizontally layered, fine-grained lacustrine and fluviatile sand deposits. A dip slip component of 5 cm reveals the minimum absolute displacement along the faults. The conjugate faults join up at depth into a single listric fault surface, which successively shallows with increasing depth. 3 m to the west the fault appears to be linked with a set of sand dike intrusions. The sand dikes are subvertical, and thin downward. Dike orientations reveal the same NNW-SSE striking trend as the adjacent normal faults and range in thickness from 6 to 15 cm. The dike fillings consist of fine
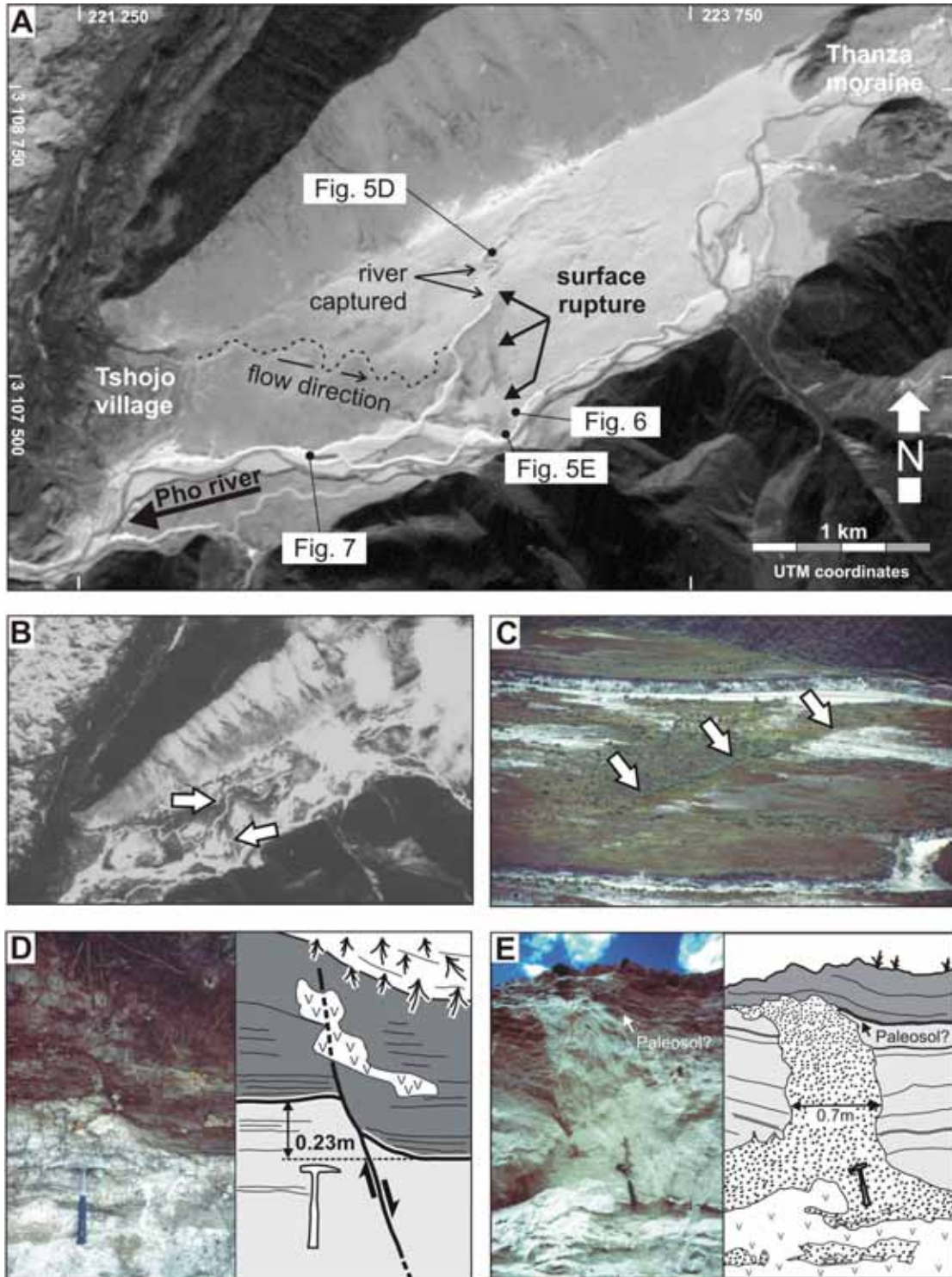
Figure 5. Tshojo plain. (a) IRS 1D satellite image (January 1996, 5 m resolution) of the Tshojo plain and the Tshojo surface rupture. Note deflection of the flow course of the local rivers. (b) Corona satellite image (January 1967, 4 m resolution) of the Tshojo plain and the Tshojo surface rupture. Deflection of the local river courses is the same as 1996. (c) Field photograph of the Tshojo surface rupture viewed toward SSE. (d) Outcrop at the northern termination of the surface rupture revealing a displaced A horizon, viewed toward south. (e) A 0.7 m thick clastic dike that coincides with the surface rupture and indicates strong liquefaction in depth, viewed toward north.
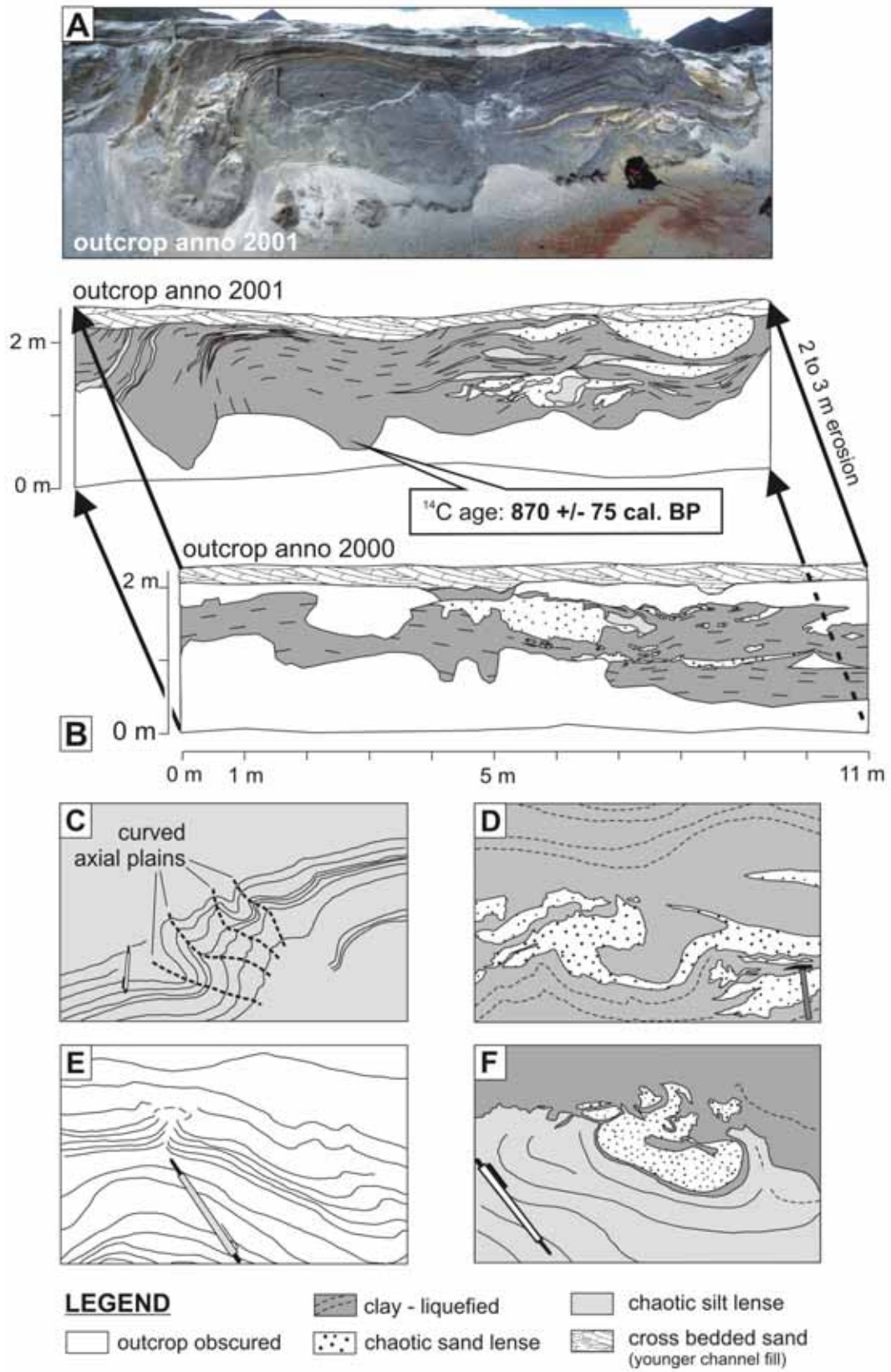
Figure 6

sand similar to that of the host sediment. Offset of host sediment along the margins of the dikes occurs and a maximum offset of about 5 cm has been observed (Figure 7). The upper ends of some dikes inject discordantly into the host sediment and locally drag the sedimentary layering of the host walls upward for a few centimeters indicating rapid injection from below [*Stewart et al.*, 2002]. The dikes are sealed by a ~50 cm thick horizontal sand layer. Both dikes and faults cut through centimeter-thick sand silt horizons with intercalated organic rich layers; a sediment sequence which we interpret as immature soils buried by repeated overbank sedimentation.

3.1.3. Clastic Dike (Intruded Gravels)

[18] Figure 5e shows a clastic dike, situated 1 km east of the complex convolute folds in a stratigraphical higher position. The clastic dike originates from a gravelly sandy source bed and breaks through a ~2 m thick fine grained cap of silty sand. The thickness of the source bed of around 1 m is a minimum estimate only, as its lower boundary is not exposed. The fine grained cap passes into a 0.3 m thick zone of immature cm thick soil horizons alternating with centimeter-decimeter thick sand layers. The clastic dike has parallel-sided walls, a thickness of ~0.7 m and a length of 1.4 m. The dike fill material is graded, fining upward from fine gravel to coarse and finally fine sand. The shape of the dike is tabular and the fluidized sediment most probably vented to the surface and was deposited on top of a ~4– 5 cm thick, dark colored, organic layer, which we interpret as a paleosol. The sand cone that resulted from such venting is not clearly identifiable because of the almost similar grain size of vented material and the fine grained sand that subsequently formed during overbank sedimentation.

3.1.4. Interpretation of Soft Sediment Deformation Features in the Tshojo Plain

[19] The amplitude and the complexity of the convolute folds, the width of the clastic dike, and the occurrence of the normal faults with parallel sand injections cannot be attributed to syndepositional or periglacial processes, but instead we argue for a seismic origin in the following:

[20] The fact that convolute folding (1) intensifies with embankment depth (as evident by comparing the outcrop situation of 2000 with 2001 in Figure 6) and (2) continues laterally beneath the undistorted Tshojo plain sediments eliminates in our opinion the significance of river level fluctuations, alluvial flooding or bed shear as possible trigger mechanisms for liquefaction. We found no evidence of sudden sediment loading or storm processes that could be responsible for the described pattern of complex convolute folding. Water table fluctuations, although capable of inducing liquefaction in susceptible sediments, cannot account for the meter-scale fold amplitudes or the "nappe

folds", the convolute lamination and the strongly curved axial plains which imply horizontal stress. Although small-scale folding resembles classic convolute folds [e.g., *Lowe*, 1975; *Mills*, 1983; *van Loon*, 1992; *Owen*, 1996], the scale and observed complexity of the folding pattern require an alternative explanation. Complex convolute folding in lacustrine and fluvio-lacustrine sediments with meter-scale fold amplitudes similar to the Tshojo situation has been described from the Aptian Codó formation, northern Brazil [*Rossetti and Góes*, 2000] or the lower Spiti Valley, Himalaya [*Mohindra and Bagati*, 1996] where, in both cases, strong seismic shaking was the cause for these deformation structures.

[21] Seismically induced liquefaction causes a volume decrease within the source bed of the liquefied layer, which can result in the development of normal faults in the overlying sediments [e.g., *Rodriguez-Pascua et al.*, 2000; *Rossetti and Góes*, 2000; *Moretti*, 2000]. We suggest this mechanism as the cause for complex convolute folding and normal faulting within the Tshojo sediments and expect escaping water-sediment mixtures from the liquefied source bed to be responsible for the adjacent sand injections (Figure 7). The parallelism of sand dikes and adjacent normal faults as well as the injection of sand along joints is typical for seismically induced formations as shown by *Bartholomew et al.* [2002] and *Rodriguez-Pascua et al.* [2000]. Downward thinning observed in seismically induced sand injections is explained by *Rodriguez-Pascua et al.* [2000] by lateral sand flow. The sand injections whose widths exceed several centimeters and whose heights exceed 1 m and cut soil horizons that are clearly much younger than the source zone of the injections generally eliminates the possibility of syndepositional dewatering processes as cause for sand injections [*Obermeier*, 1996, p. 8]. Moreover, and in contrast to a nonseismic origin, offset of host sediment along the margins of our sand injections (Figure 7) is only known for seismically induced sand dikes [*Bartholomew et al.*, 2002].

[22] A mechanism to explain the clastic dike with a width of 0.7 m and intruded by gravels (Figure 5e) is lateral spreading which again implies strong earthquake shaking [*Obermeier*, 1996; *Valera et al.*, 1994]. Lateral spreading is caused by an increased pore water pressure during ground shaking which decreases the strength of granual strata at depth and huge masses of overlying soil can thus shift horizontally in the form of laterally moving landslides [*Obermeier*, 1996]. At the same time sediment from the liquefied layer below may vent through fissures to the surface and form clastic dikes. Lateral spreading has been proposed to be associated with strong earthquakes, forming clastic dikes with similar and even greater width in other

---

Figure 6. Complex convolute folding in the Tshojo plain. (a) Large-scale folds superimposed on small-scale convolutions. Note vertically dipping fold limb in the left part of the picture. View toward NE, rucksack for scale. (b) Outcrop situation in two subsequent years. Radiocarbon dating on base of outcrop gives age constraints. (c–d) Details of complex convolute folding, pencil or hammer for scale. Figure 6c shows distorted fold with irregular morphology and size. Axial plains are inclined at different angles within the same fold. Figure 6d shows "nappe fold" developed where coarse sand is interbedded with clay, indicating horizontal displacement. (e) Disrupted and dragged silt layer due to vented water-sediment mixture. (f) Pseudonodules formed by sinking into underlying clay deposit due to reversed density gradients.
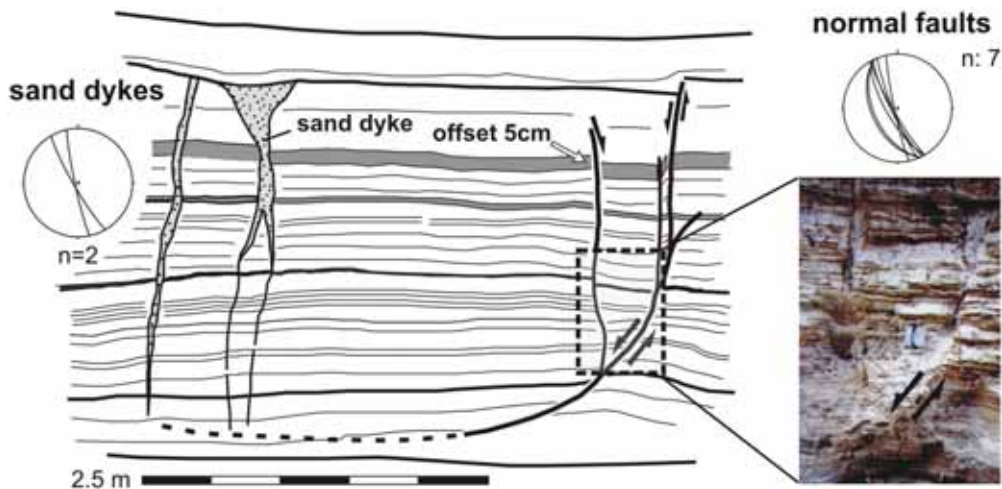
Figure 7. Normal faulted sediments and sand injections in the Tshojo plain. Centimeter-scale displacement of the host sediment occurs along normal faults and sand dike margins. Faults and dikes strike parallel to the brittle D2 fault group. View is toward north.

regions in the world, e.g., the Wabash Valley seismic zone, the New Madrid Zone [*Obermeier*, 1996] and in south central Indiana [*Munson et al.*, 1995] and dikes as much as 0.3 m wide have been associated with the great Assam earthquake west of the Shilong plateau [*Sukhija et al.*, 1999]. In the Tshojo plain lateral spreading may have been facilitated by free surfaces formed by the riverbanks of the Dota and Pho river in the west and the south, respectively, thus reducing resistance to lateral movement (Figure 5a). As lateral spreading occurs on nearly level ground (ground surface inclination of the plain: 0.4°) and the fissures were intruded by gravels, we dismiss gravitational sliding and artesian conditions as possible causes.

[23] The Tshojo plain is ice free since the beginning of the Holocene and is situated well below the recent limit of discontinuous permafrost [*Meyer et al.*, 2001; *Iwata et al.*, 2003], ruling out dead ice content or permafrost processes to produce ice wedged casts or cryoturbation capable to mimic features of earthquake origin.

[24] In summary, we propose that seismically induced ductile deformation of water saturated sediments in depth was responsible for complex convolute folding which in turn caused brittle deformation and lateral spreading in the overlying strata of the plain. We thus expect the liquefied source bed to extend at least 1.2 km in E-W direction (Figure 5a). It is this stratigraphical and spatial association of deformation structures that strengthens the argument of their seismic origin.

3.2. Tshojo Surface Rupture and Lineament Interpretation for West Bhutan

[25] The most conspicuous evidence for strong earthquakes in the Lunana area is a 6.8 km long surface rupture cutting the Tshojo plain in N-S direction and continuing farther south into the glacially overprinted crystalline bedrock (Figure 8). As shown below, the sharp lineament spatially coincides with both the normal faulted sediments and the clastic dike described above and influences the flow pattern of tributary rivers in the Tshojo plain. These structures and their spatial arrangement and morphological expression are best explained as the result of a surface rupturing earthquake.

[26] The striking lineament is visible in satellite imagery and field photographs of the Tshojo area (Figures 8 and 5c). A small river flowing westward is captured by the surface fault and deflected into a southern direction, while the river coming from the Tshojo village is forced to flow eastward toward the fault zone and apparently upstream (Figure 5a). We use IRS-1D satellite imagery (5 m resolution) to trace this lineament for another 3.5 km toward the south into a deglaciated, narrow cirque. From detailed field mapping we discard toppling structures, ice marginal or subglacial deposits and topographic ridges. The lineament runs straight, shows no overstepping and disappears south of the Pho river for about 1 km where it crosses the flanks of steep Pleistocene moraines. Topographic shadowing and creeping soil obscure the trace in this area. At the bottom of the cirque, three shorter lineaments, between 1 km and 1.5 km in length, run subparallel to this fault and are interpreted as smaller fault segments linked with the master fault at greater depth. An outcrop situated in the Tshojo plain at the northern termination of the rupture reveals normal-faulting kinematic for this part of the surface fault (Figure 5d). The outcrop exposes young alluvial sands and the lower part of the A horizon of the modern soil. They are vertically displaced for about 23 cm by a sharp fault plane which strikes in N-S direction and dips steeply toward the west. Fault orientation and kinematics are the same as for the brittle D2 faults in Eastern Lunana [*Wiesmayr et al.*, 2002]. The normal fault as exposed in the outcrop precisely coincides with the surface trace of the lineament in the
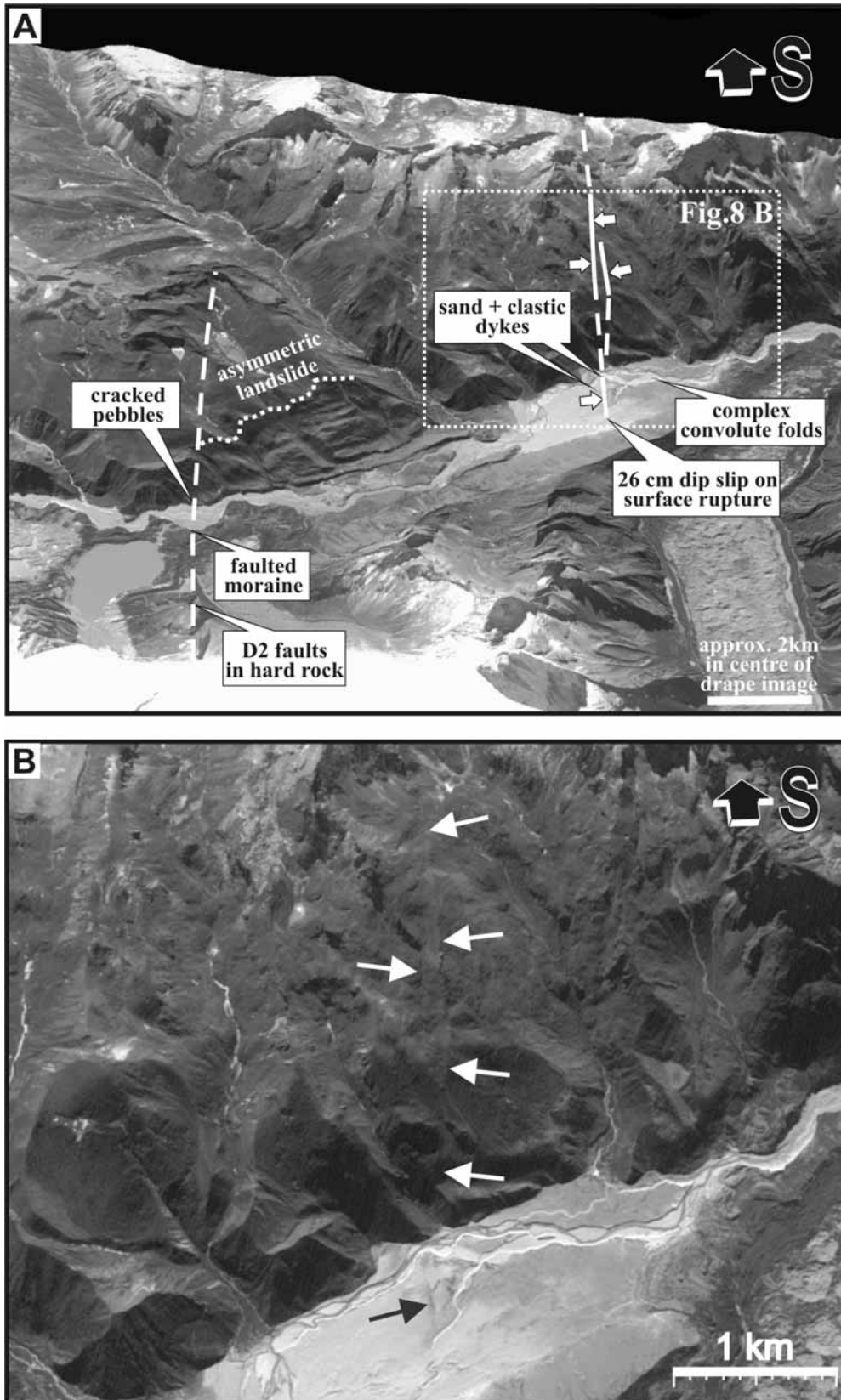
Figure 8

satellite image (Figures 5a and 8). Thus 23 cm of vertical slip occurred along the master fault rather than along secondary faults but we cannot discriminate coseismic displacement from postearthquake creep (postcoseismic creep and/or fault creep) in the outcrop.

[27] We interpret this lineament crossing the unconsolidated sediments in the Tshojo plain and continuing in the crystalline bedrock farther to the south, as one single rupture segment. The surface fault is clearly visible for about 4.5 km which is assumed as the minimum rupture length. North of the Tshojo plain there is no continuation of the surface rupture but it eventually extends as far as 2.3 km to the adjacent catchment area immediately south of the cirque where it disappears beneath an active rock glacier (Figure 8). Interpretation is hampered by the ground resolution of the satellite imagery available for this part of Eastern Lunana (Landsat TM, 30 m ground resolution), but we consider the resulting 6.8 km as a possible maximum length for the Tshojo surface fault. The 0.7 m thick clastic dike of the Tshojo plain, described above, is located directly on the surface rupture and thus may genetically be related to the faulting event (Figure 8b). By analyzing the satellite imagery and a digital elevation model (40 m resolution, generated from topographic maps) the faint trace of a second surface rupture with similar length and orientation is visible 6 km to the east (Figure 8a). The histogram of the IRS 1D satellite image has been stretched and the enhanced image was draped over the digital elevation model prior to visual examination for lineaments. This procedure facilitated interpretation as the spatial relationship of depositional and erosional elements of this glacial landscape and possible fault traces are further clarified.

[28] In order to regionally correlate the local fault pattern, we analyzed a 100 km broad area of western Bhutan on Landsat TM and IRS 1D satellite images for traceable faults that could as well be presently active in west Bhutan (Figure 9). We focused only on NW-SE to NE-SW striking lineaments as these structures are potentially active faults in the Bhutan Himalaya [*Gansser*, 1983] and correspond to the Tshojo surface rupture and the D2 fault pattern, which is the youngest fault pattern in NW Bhutan [*Wiesmayr et al.*, 2002]. Thus E-W trending structures were not included for this lineament interpretation. In western Bhutan, we observed single N-S trending lineaments with characteristic lengths of 1–10 km scattered roughly parallel to the Mo and the Pho rivers. Nevertheless, a closer examination reveals distinct zones of higher concentration and en echelon or back-to-back arrangement of these structures. Between 27.2°N and 26.9°N latitude the Pho river follows a prominent zone of N-S striking lineaments. This clear N-S alignment of lineaments disbands farther north. N-S striking

faults and fractures are pronounced again between 26.6°N and 28.0°N latitude and concentrate along the Pho and Mo rivers. Between 27.8°N and 28.0°N latitude and about 20 km south of the investigation area the faults and fractures, which are aligned along the Pho river, band into NW-SE direction to follow the course of an unnamed tributary of the Pho river. Finally these lineaments merge into the area of the N-S trending Tshojo surface rupture. The abundance of NW-SE striking lineaments north of Laya is already related to the adjacent Yadong Gulu rift.

3.3. Raphstreng and Thanza Area

3.3.1. Fractured Pebbles in a Pleistocene Kame Terrace

[29] South of the Pho river, opposite of the Raphstreng glacial lake, sediments of a kame terrace are exposed (Figures 10a and 10d). Geomorphologic mapping revealed that the outcrop is situated at the base of an extensive Pleistocene kame terrace and was once overlain by about 320 m of glacio-fluvial sediment, most of which is eroded. Over a distance of 15 m, fractured pebbles are frequent within this uncemented deposit but absent farther upstream and downstream. The poorly sorted sediment consists of subangular to rounded components ranging in size from 5 cm to 30 cm; a few boulders are about 1 m in diameter. Rounded pebbles are prevailing but subangular and rounded components were found fractured. Sand and gravel fill the space between these components and give rise to a grain-supported sediment. Locally sand and gravel forms a rather coarse matrix thus preventing components from direct grain to grain contact. The fractures occur in the coarse components only and do not propagate into the matrix. The components are composed of leucogranite and migmatite and the fracture devolpment is not favored by any preexisting foliation or metamorphic layering. Over the scale of the outcrop, fractures are subparallel to each other. The parallelism appears to be independent of the relative size of the pebbles and the space between them. Fracture surfaces are planar and fracture parallel displacement is rare with displacement of individual pebbles not exceeding a few centimeters. Most important is the clear and consistent regional trend revealed by systematic measurements of the fractures. The fractures strike predominantly NNE-SSW (Figure 10d), which is parallel to the principal shortening axis e_2 (Figure 10g) and thus in good agreement with the E-W extension and the corresponding strike-slip regime of deformation phase D2 (Figures 3 and 10g). *Eidelmann and Reches* [1992] demonstrate that seismically fractured pebbles may occur in poorly cemented conglomerates and are excellent indicators for the regional tectonic stress. The precondition are several hundred meters of sediment overburden which enables the components to fracture parallel to

---

Figure 8. Tshojo surface rupture. (a) IRS-1D satellite image (5 m resolution, 1996) draped over a digital elevation model (40 m resolution, generated from topographic maps). View is to the south. Surface rupture and liquefaction in the Tshojo plain are interpreted to be caused by an $M \geq 6$ earthquake. The trace of a second surface rupture which bounds the asymmetric landslide and coincides with the cracked pebbles, the faulted Raphstreng moraine and D2 faults in the hard rock occurs 6 km to the east. (b) Detail of the Tshojo surface rupture which cuts the young alluvial sediments north and the crystalline bedrock south of the Pho river.
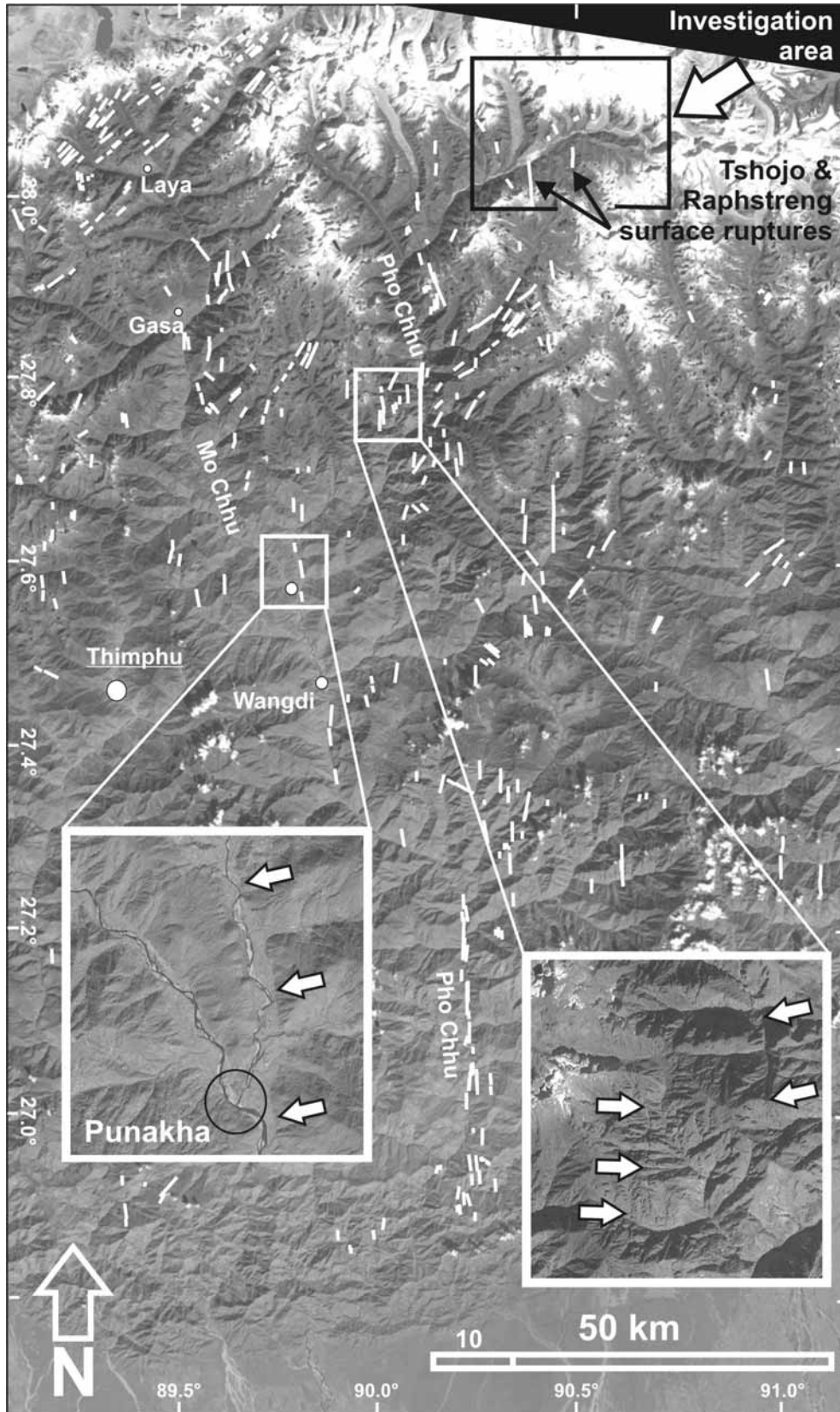
Figure 9

the largest tectonic compression (δ_{hmax}) even within matrix-supported material [*Eidelmann and Reches*, 1992].

3.3.2. Faulted Raphstreng Moraine

[30] Within a latero-frontal moraine segment of the Raphstreng glacier, a single high-angle reverse fault cuts through the diamicton and displaces an embedded glacio-fluvial sand lens for 5 cm (Figures 10e and 10f). The nonundulating fault plane dips with 68° away from the former glacier margin toward the west and reveals a fracture length of about 3.3 m (downward termination not exposed). The fault strike is parallel to the 5 m high and approximately N-S trending moraine ridge. This outcrop is situated just opposite the previously described fractured pebbles and immediately southwest of the Raphstreng glacial lake (Figure 10a). We exclude glacier push within this small single crested moraine because (1) the fault is observed to dip away from the former glacier margin whereas glacier push would preferentially produce a low-angle reverse fault that would dip toward the glacier margin [*Bennett*, 2001] and (2) within intensively deformed sediments, high-angle reverse faults may occur but are typically associated with further glaciotectonic features such as thrust related folding and thrust imbrication with parallel clast fabrics [*Humlum*, 1985; *Phillips et al.*, 2002]. The opposite is true for the Raphstreng moraine; that is, the fault cuts the sedimentary clast fabric at a high angle and glaciotectonic features are entirely missing.

3.3.3. Asymmetric Landslide

[31] South of Thanza village, a striking staircase of ice marginal deposits dips up valley at an angle of 8° over a distance of 2.5 km (Figure 11). The lateral moraines and kame terraces extend between 4350 m and 4550 m asl and were deposited during the stepwise reduction of a Pleistocene ice stream net. A primary sedimentary mechanism for depositing these ice marginal sediments with an 8° dip upstream would require a glacier flow directed up valley, which is unreasonable. Over an area of 2.4 km² approximately $40-60 \times 10^6$ m³ of quaternary sediment are affected by this asymmetric translational landslide and the well-preserved scarp is visible in the high-resolution drape image (Figure 8). The scarp and the landslide are vegetated and show no evidence for ongoing or multiple sliding events. Several generations of kame terraces and lateral moraines can be traced over the width of the landslide, proving in-block sliding rather than movement of single small clods. Processes of paraglacial resedimentation, which operate on freshly deglaciated slopes, cannot account for asymmetric in-block sliding south of Thanza village because (1) gully incision and coalescing debris cones at the valley floor, typical for paraglacial resedimentation [*Ballantyne*, 2002; *Owen and Sharma*, 1998], are lacking, (2) initial till slope gradients >27°–30° are a prerequisite for extensive slope modification during the

paraglacial period [*Curry*, 2000; *Rickenmann and Zimmermann*, 1993], but the original angle for the till-mantled slope south of Thanza village prior to sliding was well below 20° as measured in adjacent and unaffected slopes farther down valley, and (3) the angle of internal friction for the tills in Lunana varies between 35° and 43° [*Leber et al.*, 2002], further impeding gravitational sliding at this site albeit sliding may be facilitated by strong monsoonal rainfall.

3.3.4. Interpretation of Deformation Features in the Raphstreng and Thanza Area

[32] Sedimentology and geomorphology of the Pleistocene kame terrace indicate that the sediment has been transported by ice-parallel meltwater streams and was deposited at an ice-marginal position. We have no indication that the material was overridden by ice after deposition and therefore exclude glacier overburden as a mechanism for pebble fracturing. In addition, glacier overburden would not account for the consistent regional trend of the fractures and the fractured pebbles within the matrix-supported zones of the sediment. We therefore use the fractured pebbles as evidence of the regional tectonic stress, indicating the principal shortening axis e_2 to be oriented N-S and proving the seismicity along active D2 faults in the Lunana area.

[33] The high-angle reverse fault in the Raphstreng moraine may result from adjustments within the sediment body as masses of associated dead ice melt. Up thrusts caused by melting dead ice reveal three characteristics [*Sanford*, 1959; *McDonald and Shilts*, 1975]: (1) a series of reverse faults rather than a single fault form, (2) the initial high-angle reverse fault curves convex upward toward the block that was relatively downthrown to become a low-angle reverse fault, and (3) a given vertical displacement would result in a fracture length approximately twenty times the amount of the displacement. None of these characteristics apply to the thrusted Raphstreng moraine thus weakening the hypothesis of melting dead ice in the underground. With respect to the active tectonics in the Lunana area we like to consider an alternative model to deform the Raphstreng moraine. We argue that the observed thrust fault may include a considerable amount of strike-slip displacement, not obvious from this outcrop due to the absence of intersecting piercing lines. D2 faults in the adjacent crystalline rocks prove the occurrence of oblique thrust faults as a result of the conjugated strike-slip system in the Lunana area (Figures 10g and 10h). We thus speculate that the Raphstreng fault may rather be an analogue to the oblique thrust faults in the crystalline outcrops.

[34] The fractures in the pebbles of the Pleistocene kame terrace and the neighboring thrust fault in the Raphstreng moraine strike parallel to prominent D2 faults visible in the Raphstreng cirque walls 2 km to the south

---

Figure 9. Lineament interpretation of west Bhutan. Landsat TM (30 m ground resolution, 1984). N-S striking lineaments are abundant along the Pho and Mo river. At 27.8° latitude the lineaments bend into NNE-SSW orientation and follow the course of an unnamed tributary of the Pho river before merging into the investigation area with the Tshojo surface rupture.
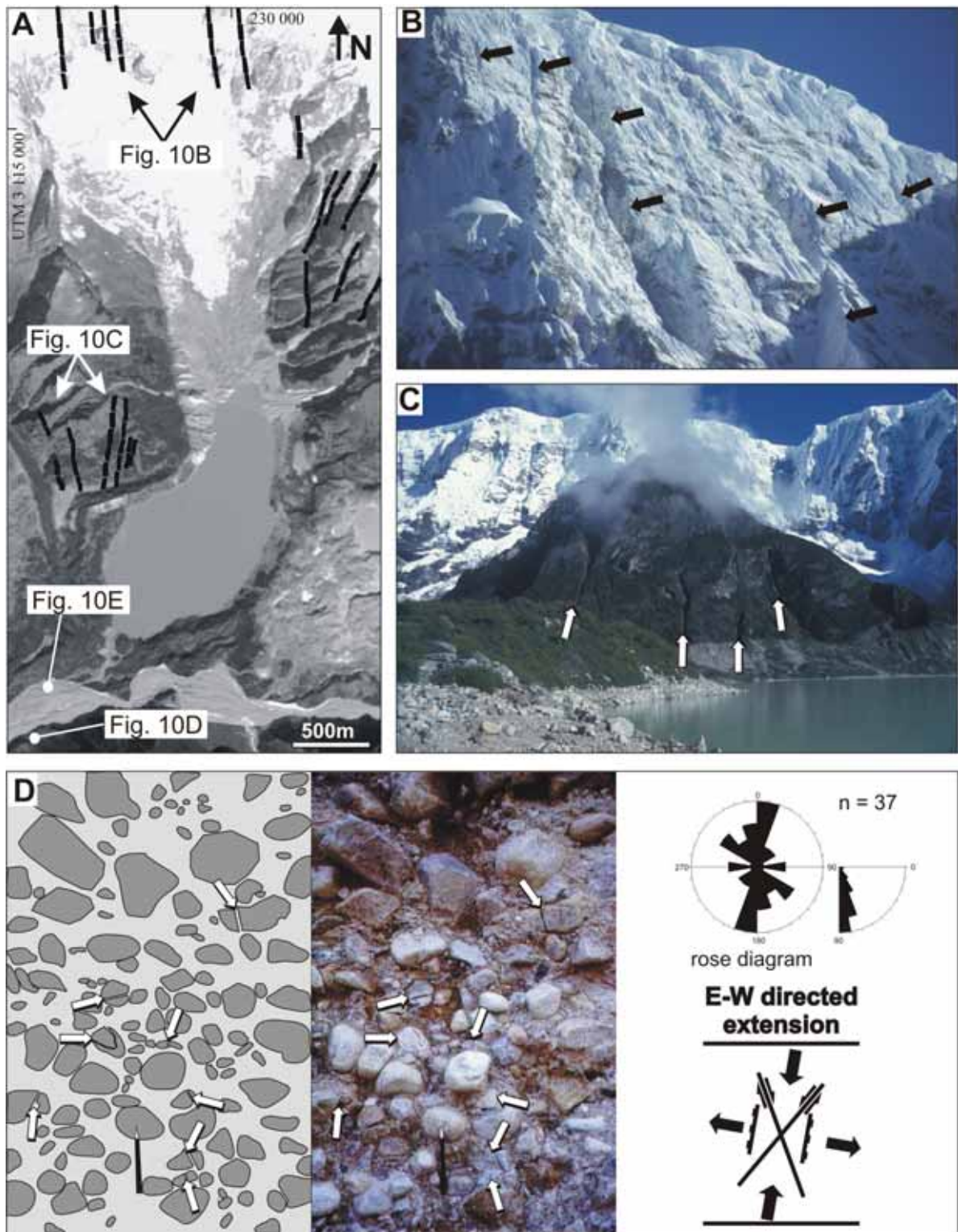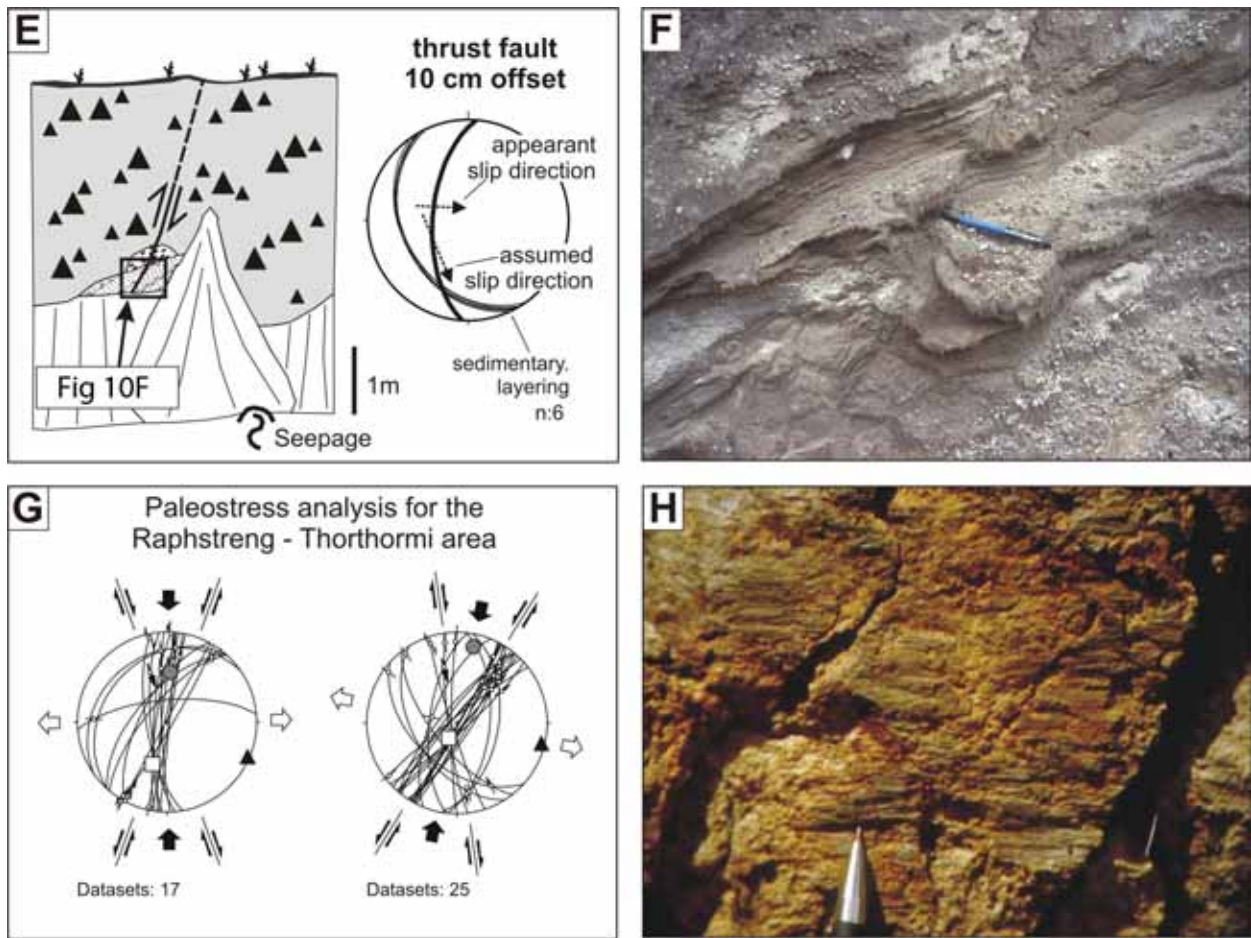
Figure 10

Figure 10. (continued)

(Figures 10b and 10c) and lie along projection of a lineament visible in the Landsat TM satellite image (Figures 8 and 9). We interpreted these deformation structures and their spatial coincidence as trace of a second surface fault crossing the Raphstreng glacial lake.

[35] This zone of active faulting marks the eastern margin of the asymmetric landslide with the highest dip-slip component of the landslide at this site (Figure 11). We thus propose seismic shaking as a potential trigger for asymmetric in-block sliding south of Thanza village, which is supported by several criteria, established by *Croizer* [1992]: (1) the ongoing seismicity in the region, (2) the presence of active faults in the area, (3) the large size of the landslide, and (4) the mechanism of failure which cannot be explained by erosional processes operating during the paraglacial period in this environment. Nevertheless geotechnical slope stability analyses are required to unequivocally prove that earthquake shaking induced slope failure at this site [*Jibson*, 1996; *Croizer*, 1992].

Figure 10. Raphstreng situation. (a) Overview of the Raphstreng glacier and glacial lake with adjacent outcrops and D2 faults in bedrock. (b) Steep cirque walls of the Raphstreng glacier with impressive D2 faults (arrows) viewed toward NE. (c) D2 faults in crystalline bedrock (arrows) above the Raphstreng lake viewed toward north. (d) Fractured pebbles in sediments of a Pleistocene kame terrace opposite of the Raphstreng Lake, viewed toward south. (e–f) A thrust faulted Holocene moraine of the Raphstreng glacier formed due to assumed oblique thrusting in a conjugated strike-slip system viewed toward north. (g) Brittle fault and paleostress analysis for the Raphstreng and adjacent Thorthormi area proving the occurrence of oblique thrust faults (bold arrows) within the set of conjugate D2 strike-slip faults. (h) Subvertical N-S trending D2 strike-slip fault in crystalline bedrock with well-developed slickenside lineation near Raphstreng glacier viewed toward west. Pencil is for scale.
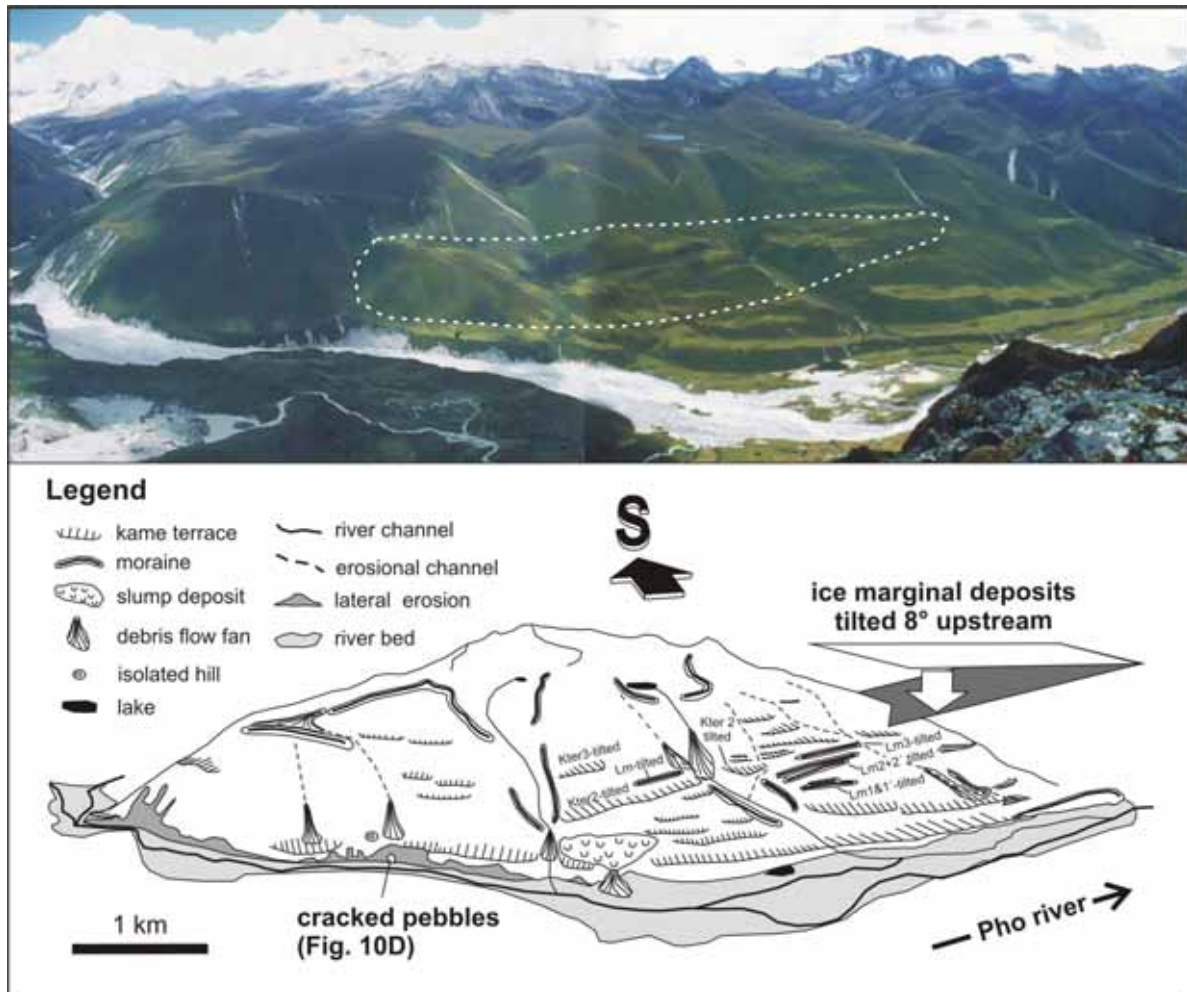
Figure 11. Asymmetric landslide south of Thanza village. About $40–60 \times 10^6$ m^3 of quaternary sediments are affected by translational sliding (white dotted outline), and seismic shaking is assumed as the most likely trigger mechanism (photograph by S. Skuk).

3.4. Seismically Active Strike-Slip Faults

[36] In Eastern Lunana, numerous unconsolidated sediments of Holocene and Pleistocene age are faulted or fractured and reveal a regionally consistent N-S trending fault pattern. The soft sediment deformation features of Eastern Lunana are associated with surface ruptures and we thus assume a seismic origin. We reemphasize the correspondence of this fault pattern with the D2 deformation phase established by *Wiesmayr et al.* [2002] from brittle fault analysis (Figure 3). The D2 faults consist of NE-SW to N-S trending sinistral strike-slip faults, NNW-SSE trending dextral strike-slip faults both comprising subhorizontal lineations, and west dipping normal faults. The set of conjugated strike-slip faults is the most prominent fault group in the D2 data set and indicates ENE-WSW extension and NNE-SSW compression. Striation on the D2 fault surfaces indicate dip-slip or strike-slip movement, respec-

tively, and do not show any crosscutting relationships. Consequently, D2 strike-slip and normal faults are interpreted to have formed contemporaneously within the same stress regime. Paleostress calculations of *Wiesmayr et al.* [2002] confirm that the D2 deformation regime is a spatially and temporally discrete event.

[37] N-S striking soft sediment deformation structures may thus be best interpreted as the result of continuous D2 deformation. In analogy to the brittle D2 N-S trending strike-slip faults we expect strike-slip faulting to be also recorded within our N-S oriented soft sediment deformation pattern. Unfortunately, we could only identify fracturing and normal faulting in the sediments that indicate only E-W extension. We argue, however, that the absence of intersecting piercing lines renders strike-slip displacement invisible in our outcrops. We speculate that the thrust faulted Raphstreng moraine may indirectly prove strike-slip movement as an oblique thrust fault within an active conjugated
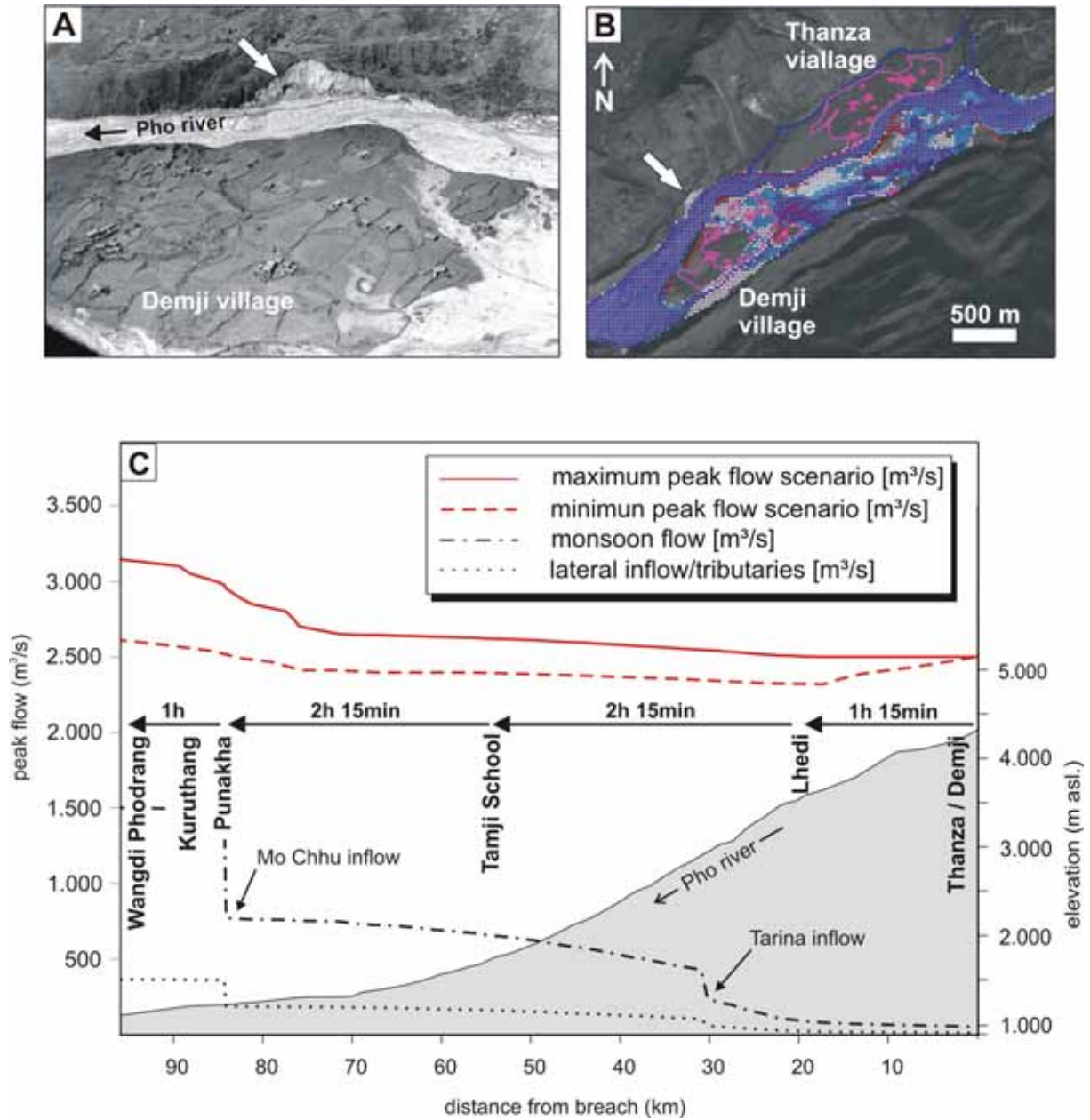
Figure 12. Calibration and simulation of flood wave scenarios based on possible outburst volumes from glacial lakes in Eastern Lunana. (a) Oblique aerial view of Demji village immediately after the GLOF on 7 October 1994. Note accumulation of coarse gravels and undercut slope in the river channel as well as flood deposits around Demji village, all indicating the dynamic behavior of the 1994 flood wave. (b) Two-dimensional back calculation of the 1994 GLOF event. Gray color indicates inundation depth < 0.3 m, no sediment transport. Light blue indicates inundation depth 0.3–1.5 m, significant sediment transport. Dark blue indicates inundation >1.5 m, significant sediment transport. Figures 12a and 12b show the good correlation between the delineated areas of inundation depth >0.3 m with significant sediment transport capacity and the 1994 GLOF event. White arrow indicates same under cut slope in both images. (c) Simulated minimum and maximum peak flow between the GLOF source and Wangdi Phodrang. The worst-case scenario uses a total outburst volume of 56×10^6 m^3 (red solid line). The peak flow is corrected for lateral and tributary inflow. The maximum monsoonal peak flow is estimated based on data from Wangdi Phodrang and Thanza gauge stations. The very low dampening and low deceleration of the flood wave peak is caused by high-relief energy and the gorge character of the Pho river between Lhedi and Tamji school.

strike-slip system rather than the result of glacier push or dead ice.

[38] Our observations and interpretations of seismically active strike-slip faults fit well with earthquake relocations and inversion results of SW Bhutan indicating strike-slip motions with midcrustal to deep-crustal depths for at least two seismic events [*Drukpa et al.*, 2006]. These authors conclude that the Indian plate is undergoing significant, transcurrent deformation throughout its depth extent, likely due to oblique convergence of the Indian-Asian collision in this region. *De and Kayal* [2003] reports a 200 km long NW-SE striking lineament which crosses the SW of Bhutan and extends to the Goalpara wedge in the NW of the Shilong plateau by cutting across the Himalayan major thrusts (Figure 1). The earthquake activity along this lineament is confined to the midcrust by strike-slip mechanism and two deep-seated earthquakes (depth >25 km) were recorded during their microearthquake survey too. Furthermore, *Kayal et al.* [1993] conducted microearthquake surveys in the eastern Himalaya between 92° and 95° longitude and found pronounced seismic activity with strike-slip focal mechanism and midcrustal to deep-crustal depths at the main boundary thrust (hypocenters >40 km: 17 out of 64, hypocenters >70 km: 6 out of 64). The epicenters are aligned roughly in N-S direction, transverse to the trend of the main boundary thrust in this part of the Himalaya orogen. In summary, seismological observations in the eastern Himalaya differ significantly from the western and central Himalaya where earthquakes are generally located above a depth of 15 km with thrust-fault focal mechanism but absent strike-slip mechanism [*Kayal*, 2001; *Khattri et al.*, 1989].

[39] Our data indicate significant active strike-slip faulting along conjugate sets of faults present within the Greater Himalaya Sequence that have been unrecognized up to now and which crosscut the Southern Tibetan Detachment System. The stress field for these conjugate sets of approximately N-S trending active faults is consistent with widespread observations throughout southern Tibet and the north Himalaya of young E-W expansion (e.g., the graben system of *Armijo et al.* [1986]). We speculate that the occurrence of these strike-slip faults mark an important transition in the geodynamics between the western and the eastern Himalaya, respectively, and strike-slip faulting might be explained by an increasing degree of oblique subduction toward the Eastern Himalaya Syntax as suggested by *Drukpa et al.* [2006].

[40] We conclude that the set of NE-SW to N-S trending sinistral strike-slip faults could extend much farther to the south, as indicated by seismological data and our lineament interpretation for NW Bhutan (Figure 9). Moreover, *Gansser* [1983] detected N-S trending lineaments, as faults and fractures from Landsat photos and field studies. He interpreted these as being seismically active fractured zones cutting the leucogranites and all previous deformation structures. In contrast to our interpretation, *Gansser* [1983] attributed N-S oriented faulting to the uplift of the "Black Mountains", a plateau-like, mountain range in central Bhutan. In our study we trace a prominent zone of

faults and fractures starting from the Tshojo surface rupture in Eastern Lunana into the adjacent southern catchment area of an unnamed tributary of the Pho river where the lineaments bend into NE-SW direction. Farther to the south the lineaments gain N-S orientation again and determine the course of the Pho river, especially south of 27.2°N latitude. Conceivably, this zone of faults and fractures may even extend farther south into the Indo-Gangetic plain and to the west of the Shilong plateau. Here, according to *Gansser* [1983] and to *Geological Survey of India* [1993], N-S lineaments and faults are detectable and may determine the flow direction of the Sankosh and Brahmaputra rivers (Figure 1).

3.5. Magnitude Estimations

[41] We apply empirical relationships between magnitude and fault parameters established by *Wells and Coppersmith* [1994] and *Pavlides and Caputo* [2004] to delimit the range of possible earthquake magnitudes for the active D2 faults in Eastern Lunana. The estimated length of 6.8 km for the Tshojo surface rupture thus corresponds to an earthquake magnitude of 6.0 (M_O [*Wells and Coppersmith*, 1994]) and 6.2 (M_S [*Pavlides and Caputo*, 2004]). Furthermore, we use the 23 cm of vertical displacement measured directly on the Tshojo surface rupture (Figure 5d), assume coseismic slip only and exclude possible postearthquake creep to assess possible maximum earthquake scenarios. Consequently, regression functions calculated by *Wells and Coppersmith* [1994] between displacement and rupture length and displacement and magnitude yield a 7 km long surface rupture and a moment magnitude of 6.4. Assessing the exact length of the Tshojo surface rupture is hampered by the resolution of the satellite imagery and may be further complicated as discontinuous surface rupturing, overstepping fault segments and blind faults could increase the length of the Tshojo surface rupture beyond the end of the continuous surface trace thus increasing magnitude estimates.

[42] Seismically triggered liquefaction features and ground failures are a function of the epicentral distance and thus only minimum magnitude estimates can be given using the liquefaction features found in the Tshojo plain or the asymmetric landslide south of Thanza village. According to *Valera et al.* [1994] the threshold magnitude to induce liquefaction effects in the most susceptible gravel deposits is about 7, whereas the threshold magnitude for sands is about 5.5. We consequently estimate the minimum magnitude for the clastic dike, which is filled with fine gravels, not to be lower than $M \leq 6$.

3.6. Dating Seismicity in Eastern Lunana

[43] Soft sediment deformation in the Tshojo plain may be best explained as the effect of a surface rupturing earthquake, leading to widespread liquefaction within the susceptible plain sediments. This seismic event is constrained in time by two observations: (1) the Corona satellite image from 1960 with the surface rupture already visible postdates the Tshojo earthquake (Figure 5b), and (2) seismically liquefied clays (complex convolute folds) which we dated to 870 years B.P. (cal ^{14}C age) predate the Tshojo

earthquake (Figure 6b). Consequently, the Tshojo earthquake occurred between 1080 A.D. and 1960 A.D.

3.7. Seismic and Glacial Hazard Potential

[44] The north Bhutan border region is not a densely populated area where an earthquake could cause a direct seismic threat to people. However, strong ground motion could trigger a dam break of moraine-dammed lakes, several of which exist in the investigated area (Figure 4). In 2001, these lakes were estimated to store about 102×10^6 m^3 of glacial meltwater [*Leber et al.*, 2002] capable of causing glacial lake outburst floods (GLOF) similar or even worse to that of the 7 October 1994 event when 20×10^6 m^3 of water was released from a glacial lake in Eastern Lunana, which caused 21 fatalities [*Watanbe and Rothacher*, 1996]. A catalogue of historical GLOFs in the Himalayas has been compiled by *Richardson and Reynolds* [2000]. According to these authors over 60% of the outburst floods were caused by ice or rock avalanches that collapsed into the lakes causing displacement waves with subsequent dam failure. Earthquake shocks may easily trigger ice or rock avalanches into glacial lakes but are additionally capable of settlement and/or piping within the moraine dams causing failure. In Eastern Lunana, several glacial lakes are in contact with steep cirque walls or hanging glaciers and each of these trigger mechanism are relevant in possible future GLOF scenarios.

[45] On the basis of detailed GLOF remediation measurements in Eastern Lunana, possible outburst scenarios range between a total volume of 13×10^6 and 56×10^6 m^3 with a peak discharge between 800 and 1800 m^3/s [*Leber et al.*, 2002]. To quantify the hazardous effects downstream, field survey data were combined with flood propagation modeling using the HEC-RAS [*Hydrologic Engineering Center, U.S. Army Corps of Engineers*, 2003] and FLO2D [*O'Brien*, 2004; *Brauner et al.*, 2003; *Leber et al.*, 2002] (Figure 12) simulation models. Erosional and depositional features in the catchment area, caused by the 1994 GLOF event, were used to calibrate these flood simulations (Figures 12a and 12b). We simulated two outburst scenarios using the minimum and maximum outburst volumes of *Leber et al.* [2002]. The results are shown in Figure 12c and the worst case scenario causes a flood wave twice the size of maximum monsoonal peak flow. The most serious impact of such outburst flood scenarios is expected to occur 80 km downstream where the valley is broad and densely populated. Between Tamji school and Kuruthang (Figure 12c), the worst case simulation indicates flooding of 42% of the infrastructure, mostly houses located in the valley floor and on fluvial terraces [*Brauner et al.*, 2003].

[46] In addition to GLOFs, if our interpretation of far south reaching active strike-slip faults is correct, $M \geq 6$ earthquakes may occur in central and southern Bhutan (Figure 9) posing a direct seismic threat to major cities in the kingdom.

4. Conclusions

[47] Paleoseismological investigations in NW Bhutan prove the occurrence of an $M \geq 6$ earthquake within a high-altitude, periglacial environment during the last millennium.

[48] Liquefaction features include an intruded clastic dike, normal faulted sediments with sand injections and complex convolute folding unequivocally point to a seismic origin and are associated with a surface rupture of about 6.8 km length. Six kilometers to the east, seismically cracked pebbles appear to be associated with the trace of a second surface rupture, a large asymmetric landslide and a faulted moraine. This second zone of assumed active faulting crosses the Raphstreng Tsho, a glacial lake that is dammed by unstable moraines only. Magnitude ≥ 6 earthquakes may trigger glacial lake outburst floods with a serious impact 80 km downstream where the valley is densely populated.

[49] Paleoseismicity occurs along the D2 fault group of *Wiesmayr et al.* [2002]: conjugate sets of faults trend NE-SW to NNW-SSE (strike-slip and normal faulting) indicating E-W extension and N-S compression and are constrained as active faults. We emphasize that significant active strike-slip faulting along these conjugate sets of faults occurs within the Greater Himalaya Sequence which have been unrecognized up to now and which crosscut the Southern Tibetan Detachment System. Our lineament interpretation reveals that N-S trending active strike-slip faults may even reach much farther to the south, at least into southern Bhutan. Our data are in agreement with micro-earthquake surveys proving strike-slip focal mechanisms in the east Himalaya and strike-slip faulting in the HHC possibly indicates an important transition in the geodynamics between the west and the east Himalaya, respectively.

[50] The glacial hazard potential in NW Bhutan requires reevaluation in the light of these new data and tectonic models of active deformation as well as seismic hazard evaluation for the entire Kingdom of Bhutan need rethinking and modification.

References

Anketell, J. M., J. Cegla, and S. Dzulynski (1970), On the deformational structures in systems with reversed density gradients, *Ann. Soc. Geol. Pologne*, *15*, 3–29.

Armijo, R., P. Tapponnier, J. L. Mercier, and T.-L. Han (1986), Quaternary extension in southern Tibet: Field observations and tectonic implications, *J. Geophys. Res.*, *91*, 803–872.

Armijo, R., P. Tapponnier, and T.-L. Han (1989), Late Cenozoic right-lateral strike-slip faulting in southern Tibet, *J. Geophys. Res.*, *94*, 2787–2838.

Ballantyne, C. K. (2002), Paraglacial geomorphology, *Quat. Sci. Rev.*, *21*, 1935–2017.

Bartholomew, M. J., M. C. Stickney, E. M. Wilde, and R. G. Dundas (2002), Late Quaternary paleoseismites: Syndepositional features and section restoration used to indicate paleoseismicity and stress-field orientations during faulting along the main Lima Reservoir fault, southwestern Montana, in *Ancient Seismites*, edited by F. R. Ettensohn, N. Rast, and C. E. Brett, *Spec. Pap. Geol. Soc. Am.*, *359*, 29–47.

Bennett, M. R. (2001), The morphology, structural evolution and significance of push moraines, *Earth Sci. Rev.*, *53*, 197–236.

Bilham, R., and P. England (2001), Plateau pop-up in the great 1897 Assam earthquake, *Nature*, *410*, 806–809.

Bilham, R., V. K. Gaur, and P. Molnar (2001), Himalayan seismic hazard, *Science*, *293*, 1442–1444.

Brauner, M., D. Leber, H. Häusler, P. Agner, T. Payer, and D. Wangda (2003), Final report of the Glacier Lake Outburst Flood (GLOF) mitigation project (2002–2003), report, 48 pp., Dep. of Geol. Sci., Univ. of Vienna, Austria.

Brenchley, P. J., and G. Newall (1972), The significance of contorted bedding in the Upper Ordovician sediments of the Oslo region, Norway, *J. Sediment. Petrol.*, *47*, 819–833.

Burchfiel, B. C., Z. Chen, K. V. Hodges, Y. Liu, L. H. Royden, C. Deng and J. Xu (1992), The south Tibetan detachment system, Himalayan Orogen: Extension contemporaneous with and parallel to shortening in a collisional mountain belt, *Spec. Pap. Geol. Soc. Am.*, *269*, 41 pp.

Burg, J. P., and G. M. Chen (1984), Tectonics and structural zonation of southern Tibet, China, *Nature*, *311*, 219–223.

Cogan, M. J., et al. (1998), Shallow structure of the Yadong-Gulu rift, southern Tibet, from refraction analysis from Project INDEPTH common midpoint data, *Tectonics*, *17*, 46–61.

Croizer, M. J. (1992), Determination of paleoseismicity from landslides, in *Landslides (Glissements de Terrain), Proceedings 6th International Symposium, Christchurch, New Zealand*, edited by D. H. Bell, pp. 1173–1180, A. A.Balkema, Brookfield, Vt.

Curry, A. M. (2000), Observations on the distribution of paraglacial reworking of glacigenic drift in western Norway, *Nor. Geogr. Tidsskr.*, 139–147.

De, R., and J. R. Kayal (2003), Seismotectonic model of the Sikkim Himalaya: Constraint from microearthquake surveys, *Bull. Seismol. Soc. Am.*, *93*(3), 1395–1400.

Dewey, J. F., R. M. Shackleton, C. Chang, and Y. Sun (1988), The tectonic evolution of the Tibetan Plateau, *Philos. Trans. R. Soc. London, Ser. A*, *327*, 301–320.

Drukpa, D., A. A. Velasco, and D. I. Doser (2006), Seismicity in the Kingdom of Bhutan (1937–2003): Evidence for crustal transcurrent deformation, *J. Geophys. Res.*, doi:10.1029/2004JB003087, in press.

Edwards, M. A., A. Pecher, W. S. F. Kidd, B. C. Burchfiel, and L. H. Royden (1999), Southern Tibet detachment at Khula Kangri, eastern Himalaya: A large-area, shallow detachment stretching into Bhutan?, *J. Geol.*, *107*, 623–631.

Eidelmann, A., and Z. Reches (1992), Fractured pebbles—A new stress indicator, *Geology*, *20*, 307–310.

Fielding, E. J., B. L. Isacks, M. Barazangi, and C. C. Duncan (1994), How flat is Tibet?, *Geology*, *22*, 163–167.

Gansser, A. (1983), *Geology of the Bhutan Himalayas*, Springer, New York.

Geological Survey of India (GSI) (1993), Bihar-Nepal earthquake, August 20th, 1988, report, edited by D. R. Nandy et al., *Geol. Surv. India Spec. Publ.*, *31*, 104 pp.

Grujic, D., M. Casey, C. Davidson, L. S. Hollister, R. Kündig, T. Pavlis, and S. Schmid (1996), Ductile extrusion of the High Himalayan Crystalline in Bhutan: Evidence from quartz microfabrics, *Tectonophysics*, *260*, 21–43.

Hodges, K. V. (2000), Tectonics of the Himalaya and southern Tibet from two perspectives, *Geol. Soc. Am. Bull.*, *112*(3), 324–350.

Humlum, O. (1985), Genesis of an imbricated push moraine, Jőfdaberkkujökull, Iceland, *J. Geol.*, *93*, 185–195.

Hydrologic Engineering Center, U.S. Army Corps of Engineers (2003), Technical reference, software supplement, 298 pp., Davis, Calif.

Iwata, S., N. Naito, C. Narama, and Karma (2003), Rock glaciers and the lower limit of mountain permafrost in the Bhutan-Himalayas, *Ann. Geomorphol.*, *130*(suppl.), 129–143.

Jackson, M., and R. Bilham (1994), Constraints on Himalayan deformation inferred from vertical velocity fields in Nepal and Tibet, *J. Geophys. Res.*, *99*, 13,897–13,912.

Jibson, R. W. (1996), Use of landslides for paleoseismic analysis, *Eng. Geol.*, *43*, 291–323.

Kayal, J. R. (2001), Microearthquake activity in some parts of the Himalaya and the tectonic model, *Tectonophysics*, *339*, 331–351.

Kayal, J. R., D. Reena, and P. Chakraborty (1993), Mircroearthquakes at the main boundary thrust in eastern Himalaya and the present-day tectonic model, *Tectonophysics*, *218*, 375–381.

Khattri, K. N., R. Chander, V. K. Gaur, I. Sarkar, and S. Kumar (1989), New seismological results on the tectonics of the Garhwal Himalaya, *Earth Planet. Sci. Lett.*, *98*, 91–109.

Langin, W. R., L. D. Brown, and E. A. Sandvol (2003), Seismicity of central Tibet from Project INDEPTH III seismic recordings, *Bull. Seismol. Soc. Am.*, *93*(5), 2146–2159.

Leber, D., H. Häusler, M. Brauner, and S. Skuk (2002), Final report on the Luggye Tsho outburst flood mitigation project, Lunana, Bhutan, report, 189 pp., Dep. of Geological Sciences, Univ. of Vienna, Vienna, Austria.

Le Fort, P. (1975), Himalayas: The collided range. Present knowledge of the continental arc, *Am. J. Sci.*, *275*(A), 1–44.

Lowe, D. R. (1975), Water escape structures in coarse-grained sediments, *Sedimentology*, *22*, 157–204.

McDonald, B. C., and W. W. Shilts (1975), Interpretation of faults in glaciofluvial sediments, in *Glaciofluvial and Glaciolacustrine Sedimentation*, edited by A. V. Jopling and B. C. McDonald, *Spec. Publ. SEPM Soc. Sediment. Geol.*, *23*, 123–131.

Meyer, M., H. Häusler, D. Leber, S. Skuk, and D. Wangda (2001), Glacial geological history and glacial lake outburst floods in Lunana, NW Bhutan, *J. Asian Earth Sci.*, *19*(3A), Special Abstract Issue, 45.

Mills, P. C. (1983), Genesis and diagnostic value of soft-sediment deformation structures: A review, *Sediment. Geol.*, *35*, 83–104.

Mohindra, R., and T. N. Bagati (1996), Seismically induced soft-sediment deformation structures (seismites) around Sumdo in the lower Spiti valley (Tethis Himalaya), *Sediment. Geol.*, *101*, 69–83.

Molnar, P., and H. Lyon-Caen (1989), Fault plane solutions of earthquakes and active tectonics of the northern and eastern part of the Tibetan Plateau, *Geophys. J. Int.*, *99*, 153–419.

Moretti, M. (2000), Soft-sediment deformation structures interpreted as seismites in middle-late Pleistocene Aeolian deposits (Apulian foreland, southern Italy), *Sediment. Geol.*, *135*, 167–179.

Munson, P. J., C. A. Munson, and E. C. Pond (1995), Paleoliquefaction evidence for a strong Holocene earthquake in south central Indiana, *Geology*, *23*, 325–328.

Nelson, K. D., and Project INDEPTH Team (1996), Partially molten middle crust beneath southern Tibet: Synthesis of project INDEPTH results, *Science*, *274*, 1684–1688.

Obermeier, S. F. (1996), Use of liquefaction-induced features for paleoseismic analysis—An overview of how seismic liquefaction features can be distinguished from other features and how their regional distribution and properties of source sediment can be used to infer the location and strength of Holocene paleo-earthquakes, *Eng. Geol.*, *44*, 1–76.

O'Brien, J. S. (2004), FLO2D user manual version 2004.10, 90 pp., FLO2D Inc. Nutrioso, Ariz.

Owen, G. (1996), Experimental soft-sediment deformation: Structures formed by the liquefaction of unconsolidated sands and some ancient examples, *Sedimentology*, *43*, 279–293.

Owen, L., and M. C. Sharma (1998), Rates and magnitudes of paraglacial fan formation in the Garhwal Himalaya: Implications for landscape evolution, *Geomorphology*, *26*, 171–184.

Pavlides, S., and R. Caputo (2004), Magnitude versus fault surface parameters: Quantitative relationship from the Aegean region, *Tectonophysics*, *380*, 159–188.

Phillips, E. R., D. J. A. Evans, and C. A. Auton (2002), Polyphase deformation at an oscillating ice margin following the Loch Lomond readvance, central Scotland, UK, *Sediment. Geol.*, *149*, 157–182.

Potter, P. E., and F. J. Pettijohn (1977), *Paleocurrents and Basin Analysis*, 425 pp., Springer, New York.

Richardson, S. D., and J. Reynolds (2000), An overview of glacial hazards in the Himalayas, *Quat. Int.*, *65/66*, 31–47.

Rickenmann, D., and M. Zimmermann (1993), The 1987 debris flows in Switzerland: Documentation and analysis, *Geomorphology*, *8*, 175–189.

Rodriguez-Pascua, M. A., J. P. Calvo, G. De Vicente, and D. Gomez-Gras (2000), Soft-sediment deformation structures interpreted as seismites in lacustrine sediments of the Prebetic Zone, SE Spain, and their potential use as indicators of earthquake magnitudes during the late Miocene, *Sediment. Geol.*, *135*, 117–135.

Rossetti, D. F., and A. M. Góes (2000), Deciphering the sedimentological imprint of paleoseismic events: An example from the Aptian Codó Formation, northern Brazil, *Sediment. Geol.*, *135*, 137–156.

Sanford, A. R. (1959), Analytical and experimental study of simple geologic structures, *Geol. Soc. Am. Bull.*, *70*, 19–52.

Searle, M. P., B. F. Windley, M. P. Coward, D. J. W. Cooper, and A. J. Rex (1987), The closing of Tethys and the tectonics of the Himalaya, *Geol. Soc. Am. Bull.*, *98*, 678–701.

Stewart, K. G., J. M. Dennison, and M. J. Bartholomew (2002), Late Mississippian paleoseismites from southeastern West Virginia and southwestern Virginia, *Spec. Pap. Geol. Soc.*, *359*.

Stüwe, K., and D. Foster (2001), $^{40}Ar/^{39}Ar$, pressure, temperature and fission track constraints on the age and nature of metamorphism around the main central thrust in the eastern Bhutan Himalaya, *J. Asian Earth Sci.*, *19*(1–2), 85–95.

Sukhija, B. S., M. N. Rao, D. V. Reddy, P. Nagabhushanam, S. Hussain, R. K. Chadha, and H. K. Gupta (1999), Paleoliquefaction evidence and periodicity of large prehistoric earthquakes in Shilong plateau, India, *Earth Planet Sci. Lett.*, *167*, 269–282.

Valera, J. E., M. L. Traubenik, J. A. Egan, and J. Y. Kaneshiro (1994), A practical perspective on

liquefaction of gravels, in *Ground failures Under Seismic Conditions*, edited by S. Prakash and P. Dakoulas, *Geotech. Spec. Publ.*, *44*, pp. 241–257, Am. Soc. of Civ. Eng., Reston, Va.

van Loon, A. J. (1992), The recognition of soft-sediment deformations as early diagenetic features—A literature review, in *Diagenesis III*, edited by K. H. Wolf and G. V. Chilingarian, pp. 135–189, Elsevier, New York.

Watanbe, T., and D. Rothacher (1996), Mountain Chronicles—The 1994 Lugge Tsho Glacial Lake outburst flood, Bhutan Himalaya, *Mt. Res. Dev.*, *16*(1), 77–81.

Wells, D. L., and K. J. Coppersmith (1994), New empirical relationships among magnitude, rupture length, rupture width, rupture area and surface dis-

placement, *Bull. Seismol. Soc. Am.*, *84*(4), 974–1002.

Wiesmayr, G., M. A. Edwards, M. Meyer, W. S. F. Kidd, D. Leber, H. Häusler, and D. Wangda (2002), Evidence for steady fault-accommodated strain in the High Himalaya; progressive fault rotation of the southern Tibet detachment system in NW Bhutan, in *Deformation Mechanisms, Rheology and Tectonics: Current Status and Future Perspectives*, edited by S. De Meer et al., *Geol. Soc. Spec. Publ.*, *200*, 371–386.

Wu, C., K. D. Nelson, G. Wortman, S. D. Samson, Y. Yue, J. Li, W. S. F. Kidd, and M. A. Edward (1998), Yadong cross structure and South Tibetan Detachment in the east central Himalaya (89°–90°E), *Tectonics*, *17*(1), 28–45.

Zhang, P. Z., et al. (2004), Continuous deformation of the Tibetan Plateau from global positioning system data, *Geology*, *32*, 809–812.

————————

M. Brauner, Geoexpert Research and Planning Gmbh, Brunhildengasse 1, A-1150 Vienna, Austria.

H. Häusler and G. Wiesmayr, Department of Geological Sciences, University of Vienna, A-1090 Vienna, Austria.

M. C. Meyer, Institute of Geology and Paleontology, University of Innsbruck, A-6020 Innsbruck, Austria. (michael.meyer@uibk.ac.at)

D. Wangda, Geological Survey of Bhutan, Ministry of Trade and Industry, Thimphu, Bhutan.